Journal Pre-proofs

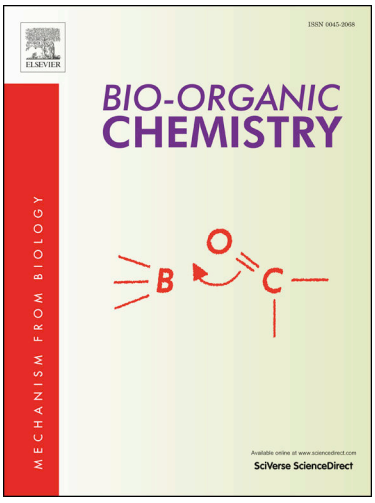

Development of 1,3-Thiazole Analogues of Imidazopyridines as Potent Positive Allosteric Modulators of $GABA_A$ Receptors

Tatyana A. Tikhonova, Irina V. Rassokhina, Eugeny A. Kondrakhin, Mikhail A. Fedosov, Julia V. Bukanova, Alexey V. Rossokhin, Irina N. Sharonova, Georgy I. Kovalev, Igor V. Zavarzin, Yulia A. Volkova

PII: S0045-2068(19)30317-7
DOI: https://doi.org/10.1016/j.bioorg.2019.103334
Reference: YBIOO 103334

To appear in: *Bioorganic Chemistry*

Received Date: 28 February 2019
Revised Date: 17 September 2019
Accepted Date: 30 September 2019

Please cite this article as: T.A. Tikhonova, I.V. Rassokhina, E.A. Kondrakhin, M.A. Fedosov, J.V. Bukanova, A.V. Rossokhin, I.N. Sharonova, G.I. Kovalev, I.V. Zavarzin, Y.A. Volkova, Development of 1,3-Thiazole Analogues of Imidazopyridines as Potent Positive Allosteric Modulators of $GABA_A$ Receptors, *Bioorganic Chemistry* (2019), doi: https://doi.org/10.1016/j.bioorg.2019.103334

This is a PDF file of an article that has undergone enhancements after acceptance, such as the addition of a cover page and metadata, and formatting for readability, but it is not yet the definitive version of record. This version will undergo additional copyediting, typesetting and review before it is published in its final form, but we are providing this version to give early visibility of the article. Please note that, during the production process, errors may be discovered which could affect the content, and all legal disclaimers that apply to the journal pertain.

© 2019 Published by Elsevier Inc.

Journal Pre-proofs

Development of 1,3-Thiazole Analogues of Imidazopyridines as Potent Positive Allosteric Modulators of $GABA_A$ Receptors

Tatyana A. Tikhonova,[†] Irina V. Rassokhina,[†] Eugeny A. Kondrakhin,[‡] Mikhail A. Fedosov,[†] Julia V. Bukanova,[§] Alexey V. Rossokhin,[§] Irina N. Sharonova,[§] Georgy I. Kovalev,[‡] Igor V. Zavarzin,[†] Yulia A. Volkova[*†]*

[†] N. D. Zelinsky Institute of Organic Chemistry, Russian Academy of Sciences, 47 Leninsky prosp., 119991 Moscow, Russia

[‡] V. V. Zakusov Institute of Pharmacology, Russian Academy of Sciences, 8 Baltiyskaya str., 125315 Moscow, Russia

[§] Research Center of Neurology, 5 By-str. Obukha, 105064 Moscow, Russia

Journal Pre-proofs

ABSTRACT

Structure–activity relationship studies were conducted in the search for 1,3-thiazole isosteric analogs of imidazopyridine drugs (Zolpidem, Alpidem). Three series of novel γ-aminobutyric acid receptor ($GABA_AR$) ligands belonging to imidazo[2,1-b]thiazoles, imidazo[2,1-b][1,3,4]thiadiazoles, and benzo[d]imidazo[2,1-b]thiazoles were synthesized and characterized as active agents against $GABA_AR$ benzodiazepine-binding site. In each of these series, potent compounds were discovered using a radioligand competition binding assay. The functional properties of highest-affinity compounds **28** and **37** as $GABA_AR$ positive allosteric modulators (PAMs) were determined by electrophysiological measurements. *In vivo* studies on zebrafish demonstrated their potential for the further development of anxiolytics. Using the OECD "Fish, Acute Toxicity Test" active compounds were found safe and non-toxic. Structural bases for activity of benzo[d]imidazo[2,1-b]thiazoles were proposed using molecular docking studies. The isosteric replacement of the pyridine nuclei by 1,3-thiazole, 1,3,4-thiadiazole, or 1,3-benzothiazole in the ring-fused imidazole class of $GABA_AR$ PAMs was shown to be promising for the development of novel hypnotics, anxiolytics, anticonvulsants, and sedatives drug-candidates.

Journal Pre-proofs

INTRODUCTION

γ-Aminobutyric acid (GABA) is the most abundant inhibitory neurotransmitter in the mammalian central nervous system (CNS) and is essential for the overall balance between neuronal excitation and inhibition [1, 2]. γ-Aminobutyric acid released from GABAergic axon terminals influences neurons *via* $GABA_A$ receptors ($GABA_ARs$), which are ligand-gated chloride ion channels that mediate fast synaptic inhibition when activated by GABA. $GABA_ARs$ are transmembrane protein complexes composed of five subunits. To date, 19 different human $GABA_AR$ subunits were identified and classified as α (α1−α6), β (β1−β3), γ (γ1−γ3), δ, ε, π, and θ [3]. The heteropentameric protein α1β2γ2 membrane composed of 2α1, 2β2, and γ2 subunits represents the most widespread adult isoform of $GABA_AR$ in the central nervous system [4-6]. Individual subunit combinations generate various $GABA_ARs$ and are responsible for distinct electrophysiological and pharmacological properties leading to specific functions [7, 8].

$GABA_AR$ bears several allosteric sites,[9-12] including those for barbiturates,[13] benzodiazepines,[14] neurosteroids,[15, 16] and avermectins [17]. $GABA_ARs$ are widely distributed in the CNS [1] and the clinical use of drugs that alter $GABA_AR$ function as anxiolytics, hypnotics, and anticonvulsants provides ample proof of the concept that the $GABA_AR$ is a verified target for medicinal chemistry. Meanwhile, multiple $GABA_AR$ subtypes that mediate these clinical effects raised the need for the development of novel highly efficient ligands for this receptor.

Benzodiazepines (BZDs) are the most important drugs for $GABA_ARs$. These compounds mainly have anxiolytic, anticonvulsant, muscle relaxant, and sedative-hypnotic effects[18]. Hence, BZDs and other chemical compounds capable of high-affinity binding to $GABA_AR$ are considered as very important therapeutic agents to treat specific diseases in the CNS. While the first ‘benzodiazepine drugs’ were 1,4-benzodiazepines (such as Diazepam), many ligands of the high-affinity BZD binding site designed more recently have a non-benzodiazepine structure. The most prominent chemotypes include a heterogeneous group of 'Z-drugs' (such as Zolpidem, Zaleplon, and Zopiclone) and pyrazoloquinolinones (such as CGS 8216). Most chemotypes comprise positive allosteric modulators (PAMs), null (silent) modulators, and negative allosteric modulators. Non-selective PAMs exhibit anticonvulsant, sedative-hypnotic, and anxiolytic activity, whereas nonselective negative allosteric modulators have proconvulsant and anxiogenic actions. Null or silent modulators, such as the BZD antidote Flumazenil, antagonize these effects *in vivo* [19]. BZDs and 'Z-drugs' act *via* binding at the extracellular interface between the γ2 subunit and adjacent α subunits [20-23].

The search for new ligands of the central BZD receptor with more selective effects compared to classical 1,4-benzodiazepines has been stimulated by evidence that specific $GABA_AR$ subtypes discriminate between BZD site ligands [24, 25]. Among various structurally diverse compounds that bind with high affinity to the BZD binding site, imidazopyridines have been extensively studied for their biological activity. BZDs and imidazopyridines exhibit essentially different receptor affinity for different $GABA_AR$ subtypes. BZDs show similar affinity for the α1, α2, α3, and α5 receptor subunits. In contrast, one imidazopyridine, Zolpidem, displays higher affinity for alpha subunits, mainly the α1 receptor subunit [26-28]. Although many structural modifications of the imidazopyridine core were proposed,[26, 28-32] the most prominent PAM effect was observed for imidazo[1,2-a]pyridines with aromatic and amide substituents (Figure 1). Among other, the FDA-approved drug Zolpidem remains a gold-standard medication (‘sleeping pill’) for

Journal Pre-proofs
treating primary insomnia,[33, 34] while Alpidem, Necopidem, and Saripidem were marketed as anxiolytic drugs. The compounds DS-1 (4-chloro-*N*-[6,8-dibromo-2-(2-thienyl)imidazo[1,2-a]pyridine-3-yl benzamide) and DS-2 (4-chloro-*N*-[2-(2-thienyl)imidazo[1,2-a]pyridine-3-yl benzamide) are PAMs selective for δ-GABA$_A$Rs. The compound DS-1 potently (low nM) enhances and directly activates GABA-evoked currents mediated by α4β3δ receptors and is the most potent known agonist of these receptors [35]. The compound DS-2 is the first PAM selective for α4/6βxδ receptors. The effects of DS2 are primarily determined by the δ subunit but are additionally influenced by the α, but not the β, subunit (α4/6βxδ > α1βxδ >> γ2-GABA$_A$Rs> α4β3) [36].

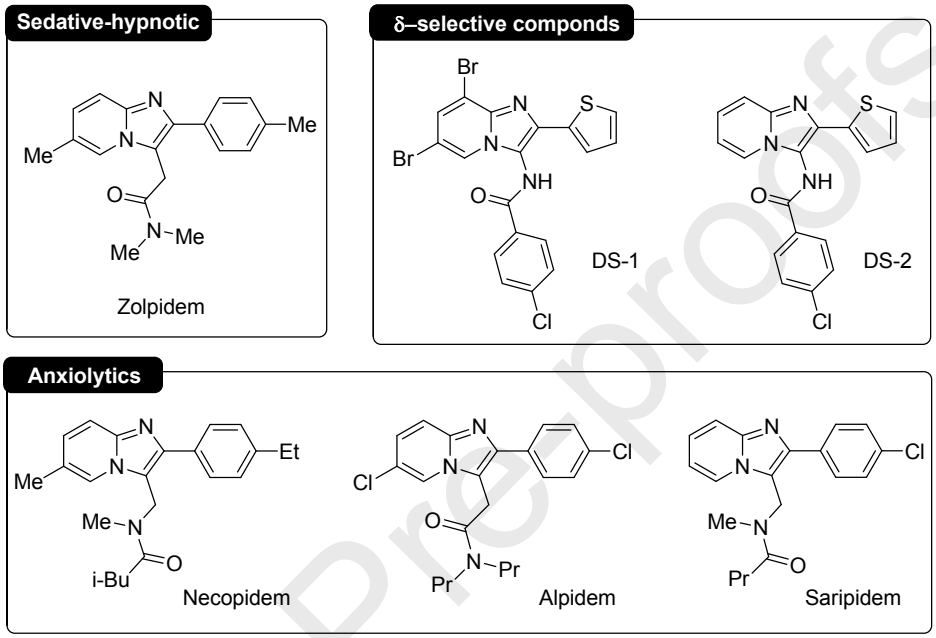

Figure 1. Overview of imidazopyridines developed as GABA$_A$Rs PAMs.

In the present paper, we report the results of our study on a new series of GABA$_A$R modulators derived by rational design from imidazopyridines. In order to obtain compounds with higher activity and taking into account that a relatively small change in the ligand structure brings about an alteration of receptor functionality, we focused our efforts on the aromatic portion of imidazopyridines and synthesized new compounds in which the pyridine ring of known imidazo[1,2-a]pyridine drugs (Zolpidem, Alpidem) is replaced by 1,3-thiazole providing imidazo[2,1-b]thiazole isosteres. Interestingly, the pharmacomodulation by replacing the aromatic moiety in drugs by sulfur-containing heterocycles was successfully used for the development of novel GABA$_A$R PAMs, such as the benzodiazepine class (leading to clotiazepam [37]) or the pyridine class (leading to SB 205384, [38] DS-1, [35] DS-2 [36]).

The pyridine/1,3-thiazole switch is expected to give rise to the following three different regioisomeric thiazole systems: imidazo[2,1-b]thiazoles (**I**), imidazo[2,1-b][1,3,4]thiadiazoles (**II**), and benzo[d]imidazo[2,1-b]thiazoles (**III**) (Figure 2). It is important to note that a few benzo[d]imidazo[2,1-b]thiazoles were described as analgesics and anxiolytics [39-41]; however, in some cases no precise data on their activity were reported in original documents, and in other cases their mechanism of action was not established and target validation was not performed. Here, we report comprehensive *in vitro* and *in vivo* studies of compounds **I-III** as GABA$_A$R PAMs. Keeping in mind that the most potent *in vivo* results for GABA$_A$R PAMs were mostly

Journal Pre-proofs

obtained for imidazopyridines with halogen substituents,[29, 42] we focused our efforts on compounds bearing chlorine, bromine, and fluorine atoms.

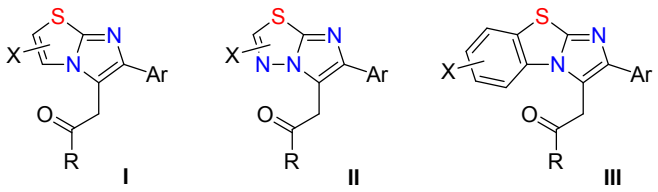

Figure 2. Three 1,3-regioisomeric thiazole systems investigated in this work.

RESULTS AND DISCUSSION

Chemistry. The structures of the compounds investigated in this study are shown in Table 1. The choice of these compounds was based on the results of the preliminary *in silico* screening of a virtual library of imidazo[2,1-b]thiazoles (see Supporting Information). We used a general synthetic approach to 1,3-thiazole-annulated heterocycles that was elaborated in our recent studies [43, 44]. Alcohol ester **1-4, 6-8,** and **11-20** and alkyl amides **5**, **9**, **10**, and **36-40** were prepared by the copper-catalyzed three-component coupling reaction of heterocyclic thioamidines with aryl aldehydes and propiolic acid derivatives (Scheme 1). This protocol was efficient for the construction of various aryl-substituted imidazo-[2,1-b]thiazoles, -[2,1-b][1,3,4]thiadiazoles, and -[2,1-b]benzothiazoles. The products yields ranged 33–78 % and were the lowest among imidazo-[2,1-b]thiazoles. High efficiency and functional group tolerance allowed the selective incorporation of aryls containing fluorine, chlorine, bromine, methyl, methoxy, trifluoromethyl, or nitro substituents into the imidazo[2,1-b]thiazole ring.

Scheme 1[a]

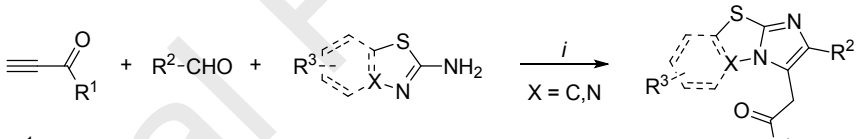

R^1 = OMe, OEt, NMe_2, NEt_2, NPr_2
R^2 = C_6H_5, *p*-MeC_6H_4, *p*-$MeOC_6H_4$, *o*-$MeOC_6H_4$, *o,p*-$MeOC_6H_3$, *p*-FC_6H_4, *o*-ClC_6H_4, *m*-ClC_6H_4, *p*-ClC_6H_4, *p*-BrC_6H_4, *o,p*-Cl_2C_6H, *m,p*-$Cl_2C_6H_4$, *p*-$CF_3C_6H_4$, *p*-$NO_2C_6H_4$
R^3 = H, Et, *iso*-Pr, CH_2OMe

1-20, 36-40

[a] *Reaction conditions*: (*i*) CuOTf•C_6H_6 (10 mol %), $Cu(OTf)_2$ (10 mol %), 4Å molecular sieves, toluene, 120 °C, 2 h.

Propiolamide (R^1 = NH_2) proved to be inefficient in the three-component coupling reaction giving unsubstituted imidazo[2,1-b]thiazole amides; multiple side reactions occurring under standard conditions. Therefore, the synthesis of compounds **21–35** was achieved from an appropriate ethyl ester by stepwise saponification and amidation of *in situ* generated acyl chloride with ammonia gas (Scheme 2).

Scheme 2[a]

Journal Pre-proofs

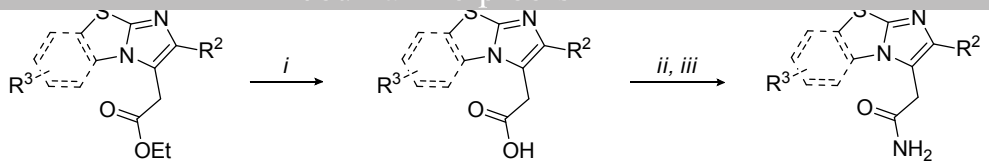

[a] *Reaction conditions*: (*i*) KOH, EtOH, rt, 10 min; (*ii*) PCl_5, CH_2Cl_2, rt, 24 h; (*iii*) NH_3, CH_2Cl_2, rt, 1 h

The overall yields over two steps were 47 to 90%. Notably, this procedure is efficient with secondary amines; alkyl amides **5**, **9**, **10**, and **36–42** can also be synthesized in quantitative yields from esters by treatment with appropriate amines.

Affinity for the benzodiazepine-binding site of GABA$_A$Rs. All synthesized compounds **1–42** were evaluated on $GABA_ARs$ at the BZD binding site. The affinity of compounds was measured using a radioligand competition binding assay by displacement of [^{3}H]Flunitrazepam binding from rat cortical membrane. Zolpidem (ZLP), a sedative-hypnotic medicine, was used as the reference compound. The corresponding inhibitory concentrations IC_{50} (IC_{50} is the half-maximal concentration of the ligand required to inhibit [^{3}H]Flunitrazepam binding by 50%) are listed in Table 1.

Journal Pre-proofs

Journal Pre-proofs

Table 1. The IC_{50} values of imidazothiazoles tested *in vitro* for [^{3}H]Flunitrazepam binding to rat cortical membranes

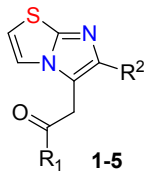

1-5

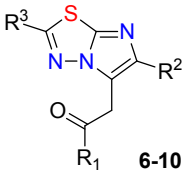

6-10

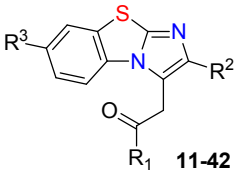

11-42

Comp.	R^1	R^2	R^3	IC_{50} value (nM)*	Comp.	R^1	R^2	R^3	IC_{50} value (nM)*
1	OMe	*p*-ClC_6H_4		>2000	**22**	NH_2	*p*-MeC_6H_4		73.0±0.2
2	OMe	*p*-$NO_2C_6H_4$		>2000	**23**	NH_2	*p*-$MeOC_6H_4$		187±6
3	OEt	*p*-ClC_6H_4		>2000	**24**	NH_2	*o*-$MeOC_6H_4$		>2000
4	OEt	*o,p*-Cl_2C_6H		>2000	**25**	NH_2	*o,p*-$MeOC_6H_3$		>2000
5	NMe_2	*p*-ClC_6H_4		839±240	**26**	NH_2	*o*-ClC_6H_4		141±5
6	OEt	*p*-ClC_6H_4	Et	>2000	**27**	NH_2	*m*-ClC_6H_4		373±6
7	OEt	*p*-ClC_6H_4	*iso*-Pr	>2000	**28**	NH_2	*p*-ClC_6H_4		10.0±0.7
8	OEt	*p*-ClC_6H_4	CH_2OMe	>2000	**29**	NH_2	*p*-ClC_6H_4	Cl	>2000
9	NMe_2	*p*-ClC_6H_4	Et	74±8	**30**	NH_2	*p*-ClC_6H_4	MeO	>2000
10	NPr_2	*p*-ClC_6H_4	Et	160±10	**31**	NH_2	*o,p*-$Cl_2C_6H_4$		178±6
11	OEt	C_6H_5		956±45	**32**	NH_2	*m,p*-$Cl_2C_6H_4$		>2000
12	OEt	*p*-MeC_6H_4		1025±41	**33**	NH_2	*p*-FC_6H_4		69±6
13	OEt	*p*-$MeOC_6H_4$		ne	**34**	NH_2	*p*-BrC_6H_4		198±8
14	OEt	*o*-$MeOC_6H_4$		>2000	**35**	NH_2	*p*-$CF_3C_6H_4$		471±5
15	OEt	*o,p*-$MeOC_6H_3$		>2000	**36**	NMe_2	*p*-MeC_6H_4		320±10
16	OEt	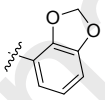		712±10	**37**	NMe_2	*o*-ClC_6H_4		6.0±0.5
17	OEt	*p*-FC_6H_4		>2000	**38**	NMe_2	*m*-ClC_6H_4		48±1
18	OEt	*p*-ClC_6H_4		>2000	**39**	NMe_2	*p*-ClC_6H_4		70±2
19	OEt	*p*-BrC_6H_4		ne	**40**	NMe_2	*o,p*-$Cl_2C_6H_4$		12.0±0.5
20	OEt	*p*-ClC_6H_4	Cl	>2000	**41**	NEt_2	*p*-ClC_6H_4		75±8
21	NH_2	C_6H_5		191±5	**42**	NPr_2	*p*-ClC_6H_4		>2000
					Zolpidem				43±1

*Each IC_{50} value is the mean of three independent measurements ± SD; ne, not established because of poor solubility of compound under experimental conditions.

We found that esters **1**–**4** and **6**–**8** of imidazo[2,1-b]thiazole and imidazo[2,1-b][1,3,4]thiadiazole series are inactive at concentrations lower than 2000 nM (Table 1), whereas the corresponding alkyl amides **5**, **9**, and **10** exhibited potency for binding to BZD site at a nanomolar level (their IC_{50} values were 839, 74, and 160 nM, respectively). The affinity of imidazo[2,1-

Journal Pre-proofs
b][1,3,4]thiadiazole **9** was just 1.7 times lower compared with the reference drug ZLP (IC_{50} = 43 nM).

In contrast, the evaluation of the benzo[d]imidazo[2,1-b]thiazole series (esters **11**–**20**) affinity revealed that compounds **11**, **12**, **13**, and **16** bearing *p*-methyl, *p*-methoxy, and *m,p*-methylenedioxy substituents at the aryl moiety have a low activity with IC_{50} ranging from 700 to 956 nM. Compounds **14** and **15** containing a methoxy substituent in the *ortho* position, as well as compounds **17**–**20** bearing halogens (F, Cl, Br) in the *para* position, proved to be inactive.

Benzo[d]imidazo[2,1-b]thiazole amides **21**–**42**, except for **24**, **25**, **29**, **30**, **32** and **42**, were found to be more potent; almost all of them displayed a nanomolar affinity below 471 nM. Compound **23** bearing a methoxy substituent in the *para* position of the aryl moiety displayed a weak activity with IC_{50} value of 187 nM, which is similar to that of unsubstituted amide **21** (IC_{50} = 191 nM). Tolyl-substituted derivative **22** exhibited an above-average potency for binding with IC_{50} = 73 nM.

Compound **28** with the *p*-ClC_6H_4 pendant showed the affinity higher to that of the drug ZLP (IC_{50} = 43 nM) with IC_{50} of 10 nM. A change in the position of chlorine atom at the aryl moiety, as well as an increase in the number of substituents in **28**, led to a decrease in its activity. Thus, the IC_{50} values of *ortho*- and *meta*-substituted analogs **26** and **27** were 141 nM and 373 nM, respectively. Compound **31** containing an o,*p*-$Cl_2C_6H_3$ substituent exhibited IC_{50} of 178 nM, while *m,p*-$Cl_2C_6H_3$-substituted **32** was inactive. The insertion of chlorine and methoxy substituents (compounds **29** and **30**) into the benzothiazole moiety of compound **28** resulted in the loss of affinity. The replacement of chlorine atom in structure **28** by other halogen substituents, such as bromine, fluorine, or trifluoromethyl (compounds **33**, **34**, and **35**), led to a decrease in its activity and an increase in IC_{50} to 69 nM, 198 nM, and 471 nM, respectively. Thus, *o*-methoxy- and *o,p*-dimethoxy substituted analogs **24** and **25** were found to be inactive. The activity of derivatives of compound **28** alkylated at the amide moiety correlates with a substituent chain length. Compound **39** containing a dimethylamide group exhibited an above-average potency for binding with IC_{50} = 70 nM, which is slightly lower than that of compound **41** with a diethylamide group (IC_{50} = 75 nM). However, an analog bearing a dipropylamide substituent was active only at concentrations above 2000 nM.

The SAR evaluation of a series of dimethyl amides **36**–**40** demonstrated that general trends in effects of their substituents at the aryl moiety on the potency for receptor binding differ from those observed for unsubstituted amides. Thus, tolyl-substituted **36** showed a weak affinity (IC_{50} = 320 nM) when compared to analog **22** (IC_{50} = 73 nM). Compound **38** *meta*-Cl substituted at the aryl moiety (IC_{50} = 48 nM) had a higher potency for binding compared to *p*-Cl-substituted compound **39** (IC_{50} = 70 nM). Amide **40** containing an *o,p*-$Cl_2C_6H_4$ substituent was among the most active compounds (IC_{50} = 12 nM). Benzo[d]imidazo[2,1-b]thiazole **37** bearing an *o*-Cl substituent at the aryl moiety was the most active compound (IC_{50} = 6 nM) of all the tested compounds, with IC_{50} being seven times lower than that of the reference drug ZLP (IC_{50} = 43 nM).

Behavioral effects on adult zebrafish and toxicity. Benzo[d]imidazo[2,1-b]thiazoles were selected for further *in vivo* evaluations based on their pronounced activity revealed by *in vitro* screening. Zebrafish displays a high homology to humans with an intact and highly conserved neurotransmitter system[45] and exhibits similar neurobehavioural phenotypes that can easily be quantified [46]. Zebrafish (*Danio rerio*) were used as an efficacious type of experimental

Journal Pre-proofs
animals, which proved to be an especially effective model organism for $GABA_AR$ ligands in *in vivo* studies [46]. The "novel tank" test was used to assess behavioral indices [47]. It was previously shown that the adult zebrafish is sensitive to the effects of known anxiolytics and sedative agents in the novel tank tests. This test, conceptually similar to the open field test in rodents, is the most extensively studied model of anxiety in the zebrafish. The novel tank test exploits the fact that adult zebrafish spend about 50% of a 5 min session in the bottom of a novel tank, an effect which is reduced by Diazepam, Buspirone, or acute ethanol treatment [48]. In accordance with the evaluation protocol fish treated with benzo[d]imidazo[2,1-b]thiazoles were exposed to the water-filled tank divided into two equal virtual horizontal portions by a line marking the outside walls. Zebrafish behavior was then processed to score behavioral endpoints, such as the time spent in top, top entries, the latency to top entry (s), and the number of freezing bouts (see Methods). We characterized drug-induced behavioral responses in adult zebrafish following their acute exposure to compounds **11**–**42**. The drug ZLP was used as the reference compound [49]. It was of particular interest in terms of the predictive value to compare the results of activity studies in the zebrafish model with the radioligand competition displacement assay data [50]. Latency to enter the upper half, transitions into the upper half of the tank, and the time spent in the upper half of the tank were found the most informative parameters for compounds **11-42** to be divided into three groups **A-C**, while freezing bouts were statistically undisruptive.

Compounds **11**, **12**, **14**–**17**, **18**, **20**, **24**, **25**, **27**, **29**, **30**, **32**, and **35** (group **A'**) with IC_{50} values higher than 370 nM (Table 1) had no pronounced effect on Zebrafish behavior (see Supporting information). There was no significant difference in latency to enter the upper half, transitions into the upper half of the tank, and the time spent in the upper half of the tank between the control group and groups of the tested compounds (some representative case studies are depicted in Figure 3A).

Amides **21**, **23**, and **31** (group **A"**) with IC_{50} ranging from 178 to 191 nM had a weak effect on adult zebrafish behavior (Figure 3A). Behavioral effects were most clearly observed upon the administration of compound **31** (IC_{50} = 178 nM), resulting in a slightly shorter time spent in the upper half of the tank, a reduced number of transitions into the upper half of the tank, and higher latency to enter the upper half compared to the control group.

Similar, but more pronounced, trends in behavioral effects were observed for compounds **13, 19, 28, 33, 34,** and **39**–**41** (group **B**, Figure 3B) with IC_{50} of 10-75 nM [51]. Compounds **13, 19**, and **28** at 1 mg/L concentrations led to a 20-fold decrease in the time spent in the upper half of the tank and a 13-fold decrease in transitions into the upper half of the tank compared to the control group. Compounds **33**, **34**, **39**, **40**, and **41** caused the reduction of the time spent in the upper half of the tank to zero along with a decrease to zero in the number of transitions into the upper half of the tank. Latency to enter the upper half in group **B** was unprecedentedly long compared with the control group.

Upon exposure to acute compounds **22** and **36**–**38** (IC_{50} = 6–320 nM, group **C**, Figure 3C), adult zebrafish showed the opposite behavior. These compounds at a 1 mg/L concentration produced anxiolytic-like behavioral effects similar to those of Zolpidem. Along with the loss of normal motor function in zebrafish, we registered long time spent in the upper half of the tank, a high

Journal Pre-proofs

number of transitions into the upper half of the tank, and low latency to enter the upper half compared to the control group. Compounds **37** and **38** were found to be most allied to Zolpidem.

It is remarkable that the observed behavioral effects in groups **B** and **C** were fully eliminated upon treatment of fish with Flumazenil,[52] which is considered to be a strong antagonist acting at the $GABA_A$Rs BZD binding site (for experimental details see Supporting Information, Figure S1). This clearly shows that the altered behavior compared to the control group upon administration of benzo[d]imidazo[2,1-b]thiazoles **13**, **19**, **22**, **28**, **33**, **34**, and **36–41** was caused by their *in vivo* binding to $GABA_A$R BZD binding sites.

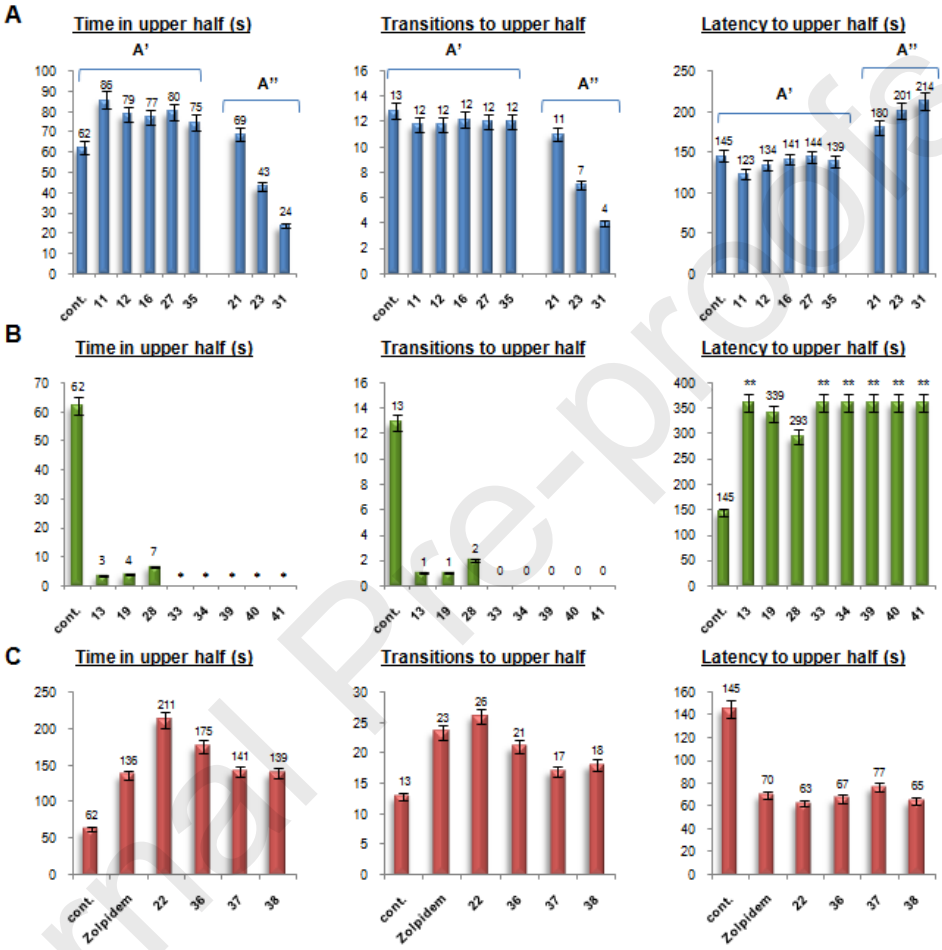

Figure 3. Effects of the studied compounds (1 mg/L, acute 20-min exposure) on adult zebrafish behavior assessed in the 6-min "novel tank" test. A group of 10 fish (approximately 50 : 50 male : female ratio) was used for each compound. The data are presented as mean ± SEM. (**A**) The results for representative compounds **11**, **12**, **16**, **27**, **35** from group **A'** (have no effects) and **21**, **23**, and **31** from group **A"** (poorly affected). (**B**) The results for compounds **13, 19, 28, 33, 34,** and **39–41** from group **B**. (**C**) The results for compounds **22** and **36–38** from group **C**.

The comparison of the results obtained using the radioligand competition displacement assay and behavioral responses in zebrafish shows that the IC_{50} values determined by the radioligand assay and the "novel tank" test corroborate each other and, hence, may be considered a predictive value, allowing a preliminary screening.

Having evaluated the *in vivo* efficacy, we assessed the safety of active compounds **13**, **19**, **21–23**, **28**, **31**, **33**, **34**, and **36–41** using the OECD "Fish, Acute Toxicity Test",[53] which is widely

Journal Pre-proofs
employed in the pharmaceutical industry to estimate the potential acute neurotoxicity of new compounds and select most promising candidates for in-depth biological testing. Compounds **13**, **19**, **21**–**23**, **31**, **33**, **34**, **36, 37**, **40**, and **41** were found to be non-toxic; one hundred percent survival of fish was observed at the maximum attainable concentrations in water (up to 47 mg/L) after a four-day exposure. Only at the maximum attainable concentrations in water (4.8 mg/L), compounds **28**, **38**, and **39** caused the loss of normal motor function in 100% of the tested zebrafish, leading to death in 2/7-3/7 animals after two days. Therefore, the lead compounds **28** and **37** were found to be safe and non-toxic.

Electrophysiological studies. Thus, we found that all three types of isosteric analogs can exert an effect on the BZD binding site of $GABA_A$Rs. Among the tested substances, the most active were imidazopyridines **28** and **37**. They showed the lowest IC_{50} values for [^{3}H]Flunitrazepam displacement activity (10 and 6 nM, respectively). Therefore, we chose these compounds and evaluated their ability to potentiate $GABA_A$R currents.

The functional properties of compounds **28** and **37** as $GABA_A$R PAMs were studied in electrophysiological experiments performed in freshly isolated rat Purkinje neurons. *In situ* hybridization studies showed a high expression of the α1, β2, β3, and γ2 mRNA in rat cerebellar Purkinje cells [54, 55]. All other $GABA_A$Rs receptor subunit genes are either absent, or expressed at much lower levels. The functional properties of $GABA_A$Rs from Purkinje cells also suggest the presence of α1, β2, β3, and γ2 subunits. These include high sensitivity to ZLP,[56, 57] indicating the presence of the α1 subunit. The type of the receptor expressed in Purkinje cells is the most common type of $GABA_A$Rs in the brain with the subunit composition α1β2γ2 [5].

We performed this set of experiments using the whole-cell patch-clamp recording and fast perfusion techniques. In all the investigated neurons, GABA application at concentrations from 1 to 300 μM at a holding potential of -70 mV elicited an inward current, whose amplitude increased with the increasing GABA concentration. The half-maximal GABA concentration for activation of $GABA_A$Rs was 5.2 ± 0.4 μM (n = 6). The modulatory effects of BZ compounds on GABA-induced currents were investigated using the co-application of 2 μM GABA (near EC_{20}) and the tested compounds in the concentration range of 10 nM–10 μM. The data were collected from 24 Purkinje neurons, all of which demonstrated the potentiation of GABA current by the tested compounds during the 2-s co-application. The sample recordings demonstrating whole-cell responses to the application of 2 μM GABA in the absence and presence of compounds **28** and **37** are shown in Figure 4.

The chloride currents were concentration-dependently increased by the application of these compounds with a maximal potentiation at about 1 μM for **28** and 3 μM for **37**. At higher concentrations, the potentiation was less pronounced, giving rise to a bell-shaped concentration effect curve for compound **28**. The threshold concentration for the potentiating effect of both compounds was 10 nM. The concentration-response relationships for the compounds under study were constructed using peak amplitudes normalized to a control response (see Methods). Compound **28** enhanced $GABA_A$R currents to a maximum of 297 ± 25% of the control current in the absence of the drug with EC_{50} of 39 ± 11 nM and a Hill slope of 1.2 ± 0.4 (n = 5-6). For compound **37**, the maximum enhancement was 198 ± 10% of the control, EC_{50} was 81 ± 24 nM, the Hill slope was 0.8 ± 0.2 (n = 8–15). The differences in EC_{50} and the maximal effects were statistically significant ($p = 5 \times 10^{-4}$ for EC_{50} and $p = 10^{-4}$ for the maximal effect). In several neurons, we performed a direct comparison of the potentiating effects of these compounds

Journal Pre-proofs

(Figure 5). This example demonstrates that the maximal potentiation of the GABA current achieved at a saturating concentration of compound **37** (3 μM) is about 200%, while an increase in the GABA response induced by the application of 1 μM compound **28** is near 300%.

To investigate the pharmacological specificity of the potentiation of the GABA-evoked currents described above, we also examined the effects of Flumazenil (Ro15-1788) that is generally considered as an antagonist acting on the BZD binding site [52]. We found that 5 μM Flumazenil completely suppressed the potentiating effect of both drugs without affecting the control response (not shown), thus indicating the involvement of the BZD binding site in the effects of compounds **28** and **37**.

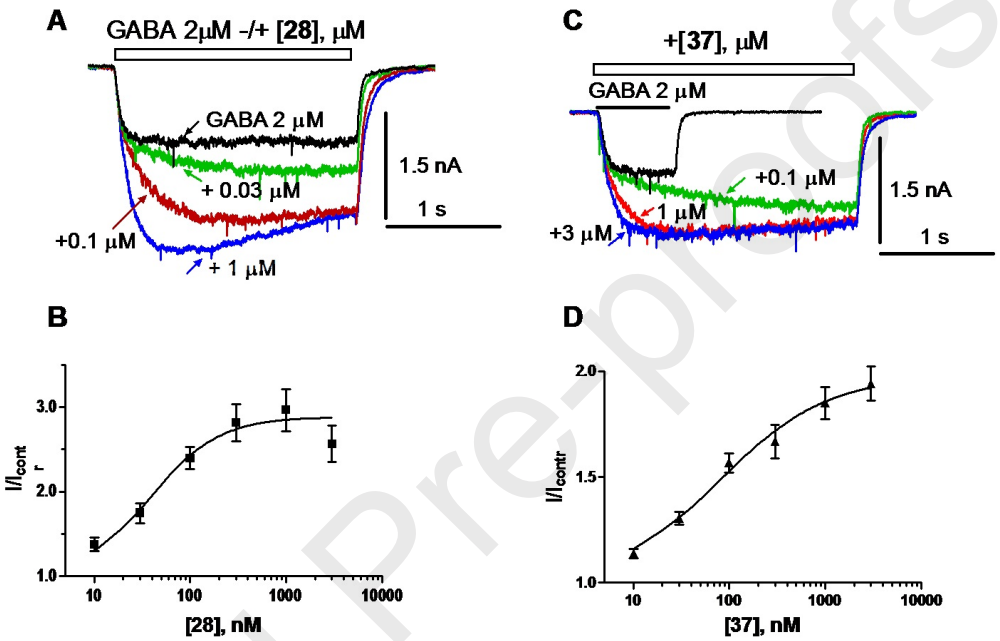

Figure 4. Potentiation of GABA-gated chloride current by various concentrations of compounds **28** and **37**. (**A**) Representative currents in acutely isolated cerebellar Purkinje cells induced by 2 μM GABA. The control current (black trace) is superimposed onto the current induced by GABA co-application at different concentrations of **28** (0.03, 0.1, and 1 μM); V_H is –70mV. Horizontal bars above the current responses show the application of 2 μM GABA and different concentrations of **28**. (**B**) Concentration-response analysis for potentiation of GABA-activated currents by **28**. Data points represent average values (mean ± S.E.M.) from 5–6 cells normalized to the current obtained under control conditions (2 μM GABA, –70 mV) and the fit by Equation 2 with the following parameters: EC_{50}=39 ± 11 nM and nH = 1.2 ± 0.4. The current amplitude was measured at the point of the maximal effect following agonist applications. (**C**) Representative currents induced by 2 μM GABA (black trace) and superimposed currents induced by GABA co-application at different concentrations of **37** (0.1, 1 and 3 μM). (**D**) Concentration-response analysis for potentiation of GABA-activated currents by **37**. Data points represent average values (mean ± S.E.M.) from 8 – 15 cells. EC_{50} = 81 ± 24 nM, nH = 0.8 ± 0.2 (*n*= 8 – 15).

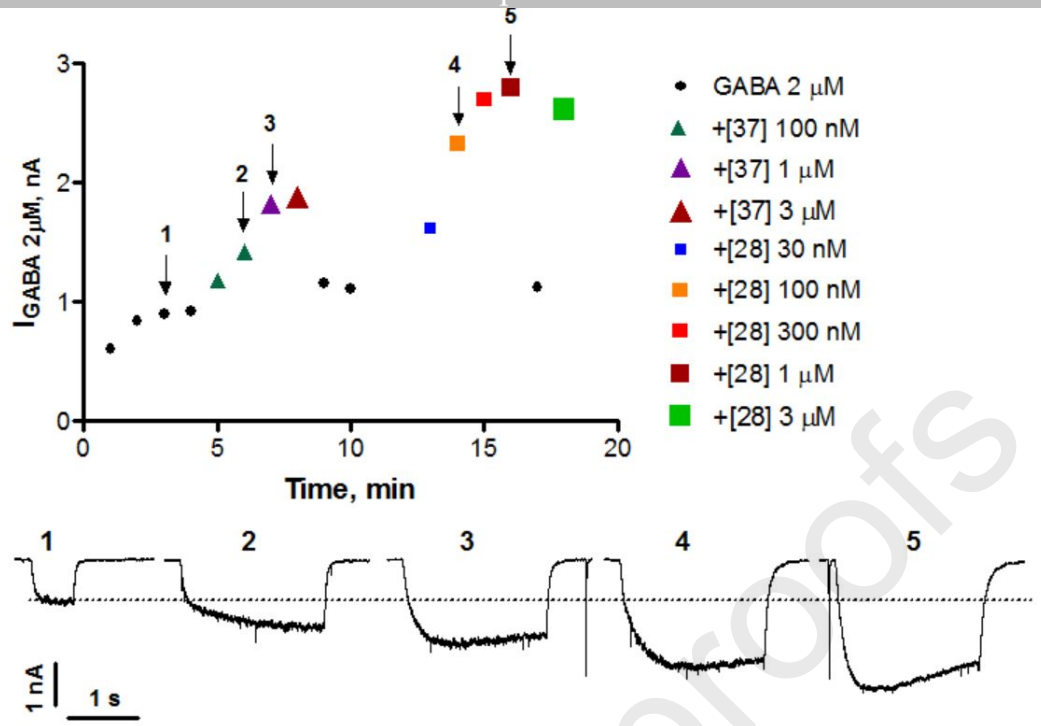

Figure 5. Comparison of the effects produced by compounds **28** and **37** on GABA currents recorded in the same neuron. Upper panel: the time course of the experiment with **28** and **37**. Each point represents the amplitude of the current induced by isolated GABA (2 μM) application (black dots) or GABA + **28** (squares)/**37** (triangles) at different concentrations (colored points, the higher the concentration, the larger the size of the symbol). Lower panel: current traces recorded at the points indicated by arrows in the upper panel. The dotted line indicates the current amplitude by GABA control (2 μM).

Therefore, our electrophysiological experiments with native $GABA_A$Rs expressed in rat cerebellar Purkinje neurons demonstrated that as with traditional BZDs, the tested compounds act by enhancing the GABAergic inhibitory drive. We found that **28** and **37** potentiate GABA currents *via* the BZD binding site. Compound **28** potentiates this GABA-induced current with the affinity similar to the estimates for the reference drug ZLP in these neurons (33 nM) [56]. However, the EC_{50} value (39 nM) for **28** was about half that of **37** (81 nM), and the maximal potentiation achieved with **28** was significantly higher than that obtained with **37** (297% and 198%, respectively). A difference in modulatory potency between these two compounds can be related to different molecular determinants responsible for the interaction of **28** and **37** with the BZD binding site.

Proposed Structural Basis for Activity of Benzo[d]imidazo[2,1-b]thiazoles and Molecular Docking. Molecular docking simulations were performed to gain insights into the structural basis for the activity of imidazo[2,1-b]thiazoles. Benzo[d]imidazo[2,1-b]thiazoles **28** and **37,** lead compounds selected on the basis of *in vitro* and *in vivo* experiments, were used as representative compounds (Figure S2). A comparison between the binding modes of these compounds and the reference drug Zolpidem was performed.

*Binding of the tested molecules (**28** and **37**) at the α(+)/γ(-) intersubunit interface.*

Journal Pre-proofs

We first docked the reference drug ZLP at the α(+)/γ(-) intersubunit interface relying rather on the shape of the binding pocket than on the specific interaction with surrounding residues. We placed the molecule in the BZD site in four different starting positions. The ZLP starting modes were defined in accordance with the direction of two different moieties (imidazopyridine ring and dimethyl amide group). Hereinafter, we refer to these modes as *i*) down-right (the imidazopyridine ring is directed downward toward the membrane and the dimethyl amide group points right toward the γ2 subunit), *ii*) down-left (the imidazopyridine ring is directed as in the down-right mode and the carbonyl-dimethyl amide group points to the left of the γ2 subunit), *iii*) up-right (the imidazopyridine ring is directed upward from the membrane and the dimethyl amide group is directed as in the down-right mode), and *iv)* up-left (the imidazopyridine ring is directed as in the up-right mode and the dimethyl amide group is directed as in the down-left mode) ones.

In each case, an extensive two-stage MCM protocol (see Methods) was used to find the minimum-energy conformations (MECs) of the ligand receptor complexes. After the convergence of the MCM trajectories, one binding mode never changes to another one, indicating that the BZD binding pocket is rather tight. The structural models of ZLP binding are shown in Figure S3 and the corresponding ligand–receptor interaction energies are given in Table 2. As it can be seen in Table 2, the down-left binding mode is energetically more favorable (–37.1 kcal/mol). Three other binding modes have similar ligand–receptor interaction energies. Most of the residues of the α1 and γ2 subunits, which were identified in the extensive mutational studies [58-62] as affecting ZLP efficacy, strongly contribute to ligand–receptor interactions in all found MECs (Figure S3 A-D).

Table 2. Energies (kcal/mol) of the ligand–receptor interaction corresponding to different binding modes of the tested ligands*

Molecule	Down-right	Down-left	Up-right	Up-left
Zolpidem	- 31.8	- 37.1	- 33.1	- 32.5
28	- 35.0	- 37.5	- 33.5	- 37.1
37	- 26.6	- 27.6	- 37.8	- 34.2

*Down-right (the imidazopyridine ring is directed downward toward the membrane and the dimethyl amide group points right toward the γ2 subunit), Down-left (the imidazopyridine ring is directed as in the down-right mode and the carbonyl-dimethyl amide group points to the left of the γ2 subunit), Up-right (the imidazopyridine ring is directed upward from the membrane and the dimethyl amide group is directed as in the down-right mode), and Up-left (the imidazopyridine ring is directed as in the up-right mode and the dimethyl amide group is directed as in the down-left mode)

To dock the tested molecules (**28** and **37**) into the BZD pocket, we initially superimposed their C_4 and C_{15} atoms (Figure S32A) onto the same atoms of ZLP in the four found MECs of ZLP-receptor complexes (Figure S3A–D). Then, the two-stage MCM protocol was again employed to find the MECs of the ligand-receptor complexes. Hereinafter, we refer to the binding modes of the tested molecules as accepted for ZLP. As in the case of the ZLP binding, the starting modes

Journal Pre-proofs
never change to other ones. The energies of ligand–receptor interactions evaluated for different binding modes of the tested molecules are given in Table 2. It is evident that the down-left and up-left MECs are more favorable for the binding of molecule **28** in the BZD pocket. For molecule **37**, the up-right binding mode is the most favorable one. The MECs of the ligand receptor complexes in these binding modes are shown in Figure 6.

The interaction energy of molecule **37** in the up-right mode is higher (in absolute values) than the energy of ZLP in the same mode (–37.8 *vs* –33.1 kcal/mol). The main difference is associated with an increase in the contribution of van-der-Waals interactions to the energy (–34.9 *vs* –31.6 kcal/mol) due to the stronger interactions between aromatic residues and the benzo[d]imidazo[2,1-b]thiazole core of molecule **37**. The set of residues involved in ligand–receptor interactions is essentially the same in both cases (Figures 6A and S3C).

In the BZD pocket, tested molecule **28** forms energetically more favorable contacts in the up-left mode (–37.1 *vs* –32.5 kcal/mol) compared to ZLP (Table 2). In this case, the energy gain is associated with an increase in the contribution of both van-der-Waals (–34.9 *vs* –31.9 kcal/mol) and electrostatic (–2.1 *vs* –0.6 kcal/mol) interactions. The interaction energies of molecules **28** and ZLP bound in the down-left modes have similar values (Table 2). The sets of residues, which essentially stabilize molecule **28** and ZLP in the binding site, are basically the same in both the binding modes (Figures 6B,C and S3B,D). In the up-left mode the benzo[d]imidazo[2,1-b]thiazole core of molecule **28** provides stronger interactions with surrounding aromatic residues. For example, the energy of interaction of Phe77 (γ_2, loop D) and Phe100 (α1, loop A) with molecule **28** is –6.3 and –1.1 kcal/mol, respectively, *vs* –4.0 and –0.5 kcal/mol in the ZLP MEC.

Journal Pre-proofs

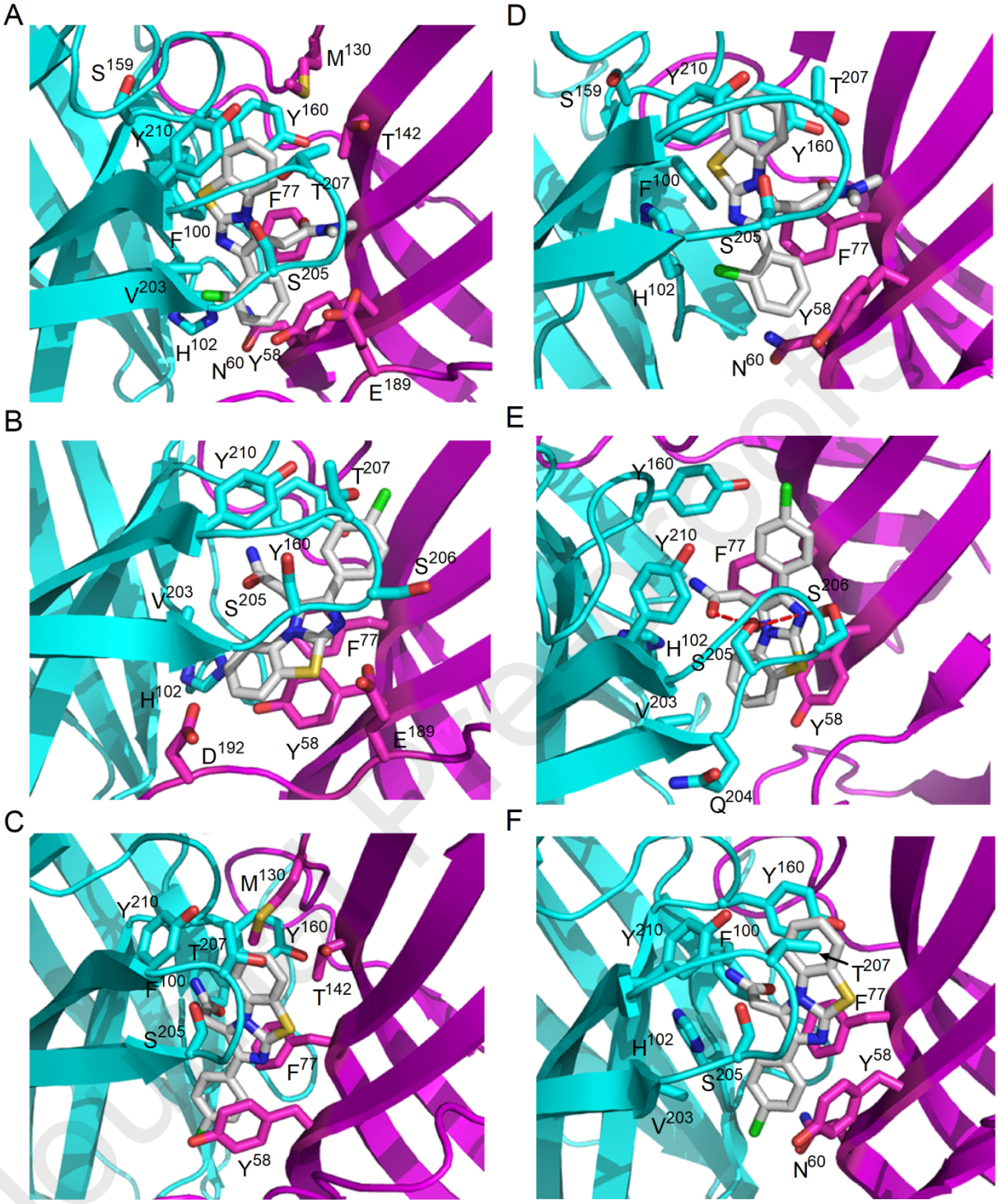

Figure 6. Favorable binding modes of the tested molecules at the α(+)/γ(-) intersubunit interface. A, D molecule **37** bound in the up-right mode. B, E and C, F molecule **28** bound in the down-left and up-left modes, respectively. In A, B and C the binding modes are shown for the α1-GlyR based model (3JAE), whereas in D, E and F the binding modes are shown for the α1β3γ2 $GABA_AR$ (6HUP). Tested molecules and side chains of residues strongly contributing to the ligand–receptor energy (> 1 kcal/mol) are represented by sticks. H-bonds are presented by red dash lines. The α1 subunit is in cyan, and γ2 is in magenta. Hydrogens are not shown.

Journal Pre-proofs
We built a homology model of $GABA_AR$ based on the structure of α1 GlyR (PDB entry 3JAE). Most recently in 2019, several new cryo-EM structures of the full-length human α1β3γ2 $GABA_AR$ in complex with GABA and the classical benzodiazepines alprazolam and diazepam become available [63]. The last ones were reconstituted in lipid nanodiscs and have undisrupted five-fold quasi-symmetrical architecture. A comparison of the cryo-EM structure of α1β3γ2 $GABA_AR$ and our homology model showed that our sequence alignment of the loop F does not correctly reflect all structural facts.

A low sequence identity in the loop F and varying sequence lengths result in many gaps in the alignment and make the last one most ambiguous among other regions of ECD of $GABA_AR$ (Fig. S2 B). The existence of the conserved V-X-V motif in the loop F, which forms a short β-strand of three residues, was not reflected in our alignment. Obviously, this misalignment cannot affect the geometry of the BZD pocket, but some interactions of the tested molecules with surrounding residues may be affected. Thus, in order to validate our models we performed the docking of the tested molecules (28 in the up-left/down-left modes and 37 in the up-right mode) to the α(+)/γ(-) intersubunit interface of the α1β3γ2 $GABA_AR$ (PDB entry 6HUP). The docking and MC minimization protocols were similar to the ones used before for the α1-GlyR based models.

The structural models of binding of the tested molecules at the α(+)/γ(-) intersubunit interface of the 6HUP structure are shown in Figures 6. The values of the ligand-receptor interaction energy of the molecules 28 and 37, bound in the up-left and up-right modes in the 6HUP structure (Fig. 6 D, F), are close to the ones obtained with the α1-GlyR based model (-35.5 *vs* -37.1 kcal/mol and -36.3 *vs* -37.8 kcal/mol, respectively). The main difference is that in the 6HUP structure residues Met130, Thr142 (loop E, γ2) and Val203, Ser206 (α1, loop C) less strongly involved in stabilization of tested molecules. The molecule 28 bound in the down-left mode more strongly interacts with the loop C (α1) residues in the 6HUP structure and forms two H-bonds with Ser205 and Ser206 (Fig. 6 E). However, in this mode compound 28 practically does not interact with residues Glu189, Val190 and Asp192 (loop F, γ2) and loses in the ligand-receptor energy compare to the α1-GlyR based model (-33.2 vs -37.5 kcal/mol).

We superimposed our homology model of the α1β2γ2 $GABA_AR$ and cryo-EM structure of the α1β3γ2 $GABA_AR$ in complex with GABA and Diazepam (DZP) [63] (Figure S4). It is easy to see that all main loops that form the BZD binding site in the interface between α1 and γ2 subunits coincide well (Figure S4 A, B). The main difference can be found in the conformations of the loops C (α1) and F (γ2). The loop F (γ2) in the 6HUP structure is more distant from the BZD pocket than in the α1-GlyR based model (Fig. S4 B). Therefore, the misalignment of the loop F residues did not affect our docking results.

Superpositions of DZP in the 6HUP structure and tested molecules **37** and **28** bound in the up-right and up-left modes, respectively, in our homology model are shown in Figure S4 C, D. Both ligands (DZP and **37**/**28**) lean on the BZD pocket floor, which is delineated by the side chain of Asn60 (γ2). The chlorine atoms in DZP and **37**/**28** molecules interact with the His102 (α1) and Asn60 (γ2) side chains. Extensive aromatic-aromatic interactions between these molecules and surrounding residues (Phe100, H102, Tyr210 in α1 and Tyr58, Phe77 in γ2) can be detected. The molecules **37** and **28** are bulkier compared to DZP. However, the positions of the ligands in general are rather well matched to each other that clearly indicates the preferred binding modes of the tested molecules at the α(+)/γ(-) intersubunit interface.

Journal Pre-proofs
Below are summarized key points of this work. $GABA_A$Rs are the site of action of a variety of pharmacologically and clinically important drugs, including BZDs barbiturates, anesthetics, neuroactive steroids, and convulsants [19, 64]. BZDs have been used clinically for more than 50 years to treat disorders such as insomnia, anxiety, and epilepsy, as well as to aid muscle relaxation and anesthesia [19]. While the first 'benzodiazepine drugs' were 1,4-benzodiazepines (such as Diazepam, Flunitrazepam), a variety of structurally diverse ligands, which bind to the BZD site, were designed more recently. Each such chemical class includes compounds that enhance (positive allosteric modulators or BZD site agonists) or reduce (negative allosteric modulators or BZD site inverse agonists) GABA-induced chloride ion flux *via* the same BZD binding site. There are approximately 20 chemical classes of ligands that bind to the BZD site of $GABA_A$R, including the structures of approximately 40 compounds. Among compounds of several chemical classes, which can interact with the BZD binding site, there are heterocycles containing an imidazole ring. Probably, imidazo[1,2-a]pyridine is the most widely used heterocyclic system of this group. It is present in marketed drugs, including anxiolytic and sedative drugs, such as zolpidem, necopidem, saripidem, alpidem, and olprinone [65].

The aim of the present study is to investigate a series of new imidazole derivatives, in which the pyridine ring of known imidazo[1,2-a]pyridine drugs (Zolpidem, Alpidem) is replaced by 1,3-thiazole providing imidazo[2,1-b]thiazole isosteres, and to establish whether these compounds can act as active ligands of $GABA_A$R BZD binding site. First, the potential GABAergic activity of these compounds was tested by investigating their ability to displace [^{3}H]Flunitrazepam from the BZD binding site of the $GABA_A$R using a radioligand competition binding assay. These radioligand binding assays were performed using a $GABA_A$R preparation from the rat cerebral cortex. [^{3}H]Flunitrazepam was found to be a photoaffinity label for the BZD sites in the brain and proved to have sufficient affinity (KD ~10 nM) to detect binding in crude homogenates.*[66]* We found that some of the tested imidazo[2,1-b]thiazoles and imidazo[2,1-b][1,3,4]thiadiazoles (**5**, **9**, and **10**) have IC_{50} in the range of 74–936 nM. More importantly, experiments revealed that benzo[d]imidazo[2,1-b]thiazoles interact with the BZD-binding site as high-affinity ligands with IC_{50} of 6 nM and 10 nM for the most active compounds **28** and **37**, respectively.

These experiments showed that 1,3-thiazole isosteres of imidazo[1,2-a]pyridines are ligands of the BZD site of $GABA_A$R. It is well established that classical BZDs, such as Diazepam or Flunitrazepam, predominantly interact with receptors composed of α1βγ2, α2βγ2, α3βγ2, or α5βγ2. They exhibit no activity against α4βγ2 or α6βγ2 receptors and weak activity against receptors containing γ1 or γ3 subunits [64]. A $GABA_A$R preparation from the rat cerebral cortex, which was used in our study, contains different $GABA_A$R isoforms. Therefore, our radioligand binding assays using classical BZD does not allow us to make a conclusion about the $GABA_A$R subtypes with which the drugs under study interact. At the same time, the discovery of a different subpopulation of $GABA_A$R subtypes in the mammalian brain suggested that the sedative-hypnotic, anxiolytic, myorelaxant, and anticonvulsant effects of BZDs may be mediated by different $GABA_A$R subtypes localized in distinct brain regions [5, 67]. The function of at least some $GABA_A$R subtypes in the brain was identified using a combined molecular genetic and pharmacological approach [68, 69]. Based on an *in vivo* point mutation strategy, α1-$GABA_A$Rs were found to mediate sedation, anterograde amnesia, and part of the seizure protection, whereas α2-$GABA_A$Rs, but not α3-receptors, mediate anxiolysis [70].

Journal Pre-proofs

Next, we evaluated the neurobehavioral effects of the newly synthesized benzo[d]imidazo[2,1-b]thiazoles **11-42** using zebrafish models. Zebrafish have become a powerful tool in neuroscience research due to due to their molecular/physiological conservation, small body size, ease of experimental manipulations *in vivo*, and rich behavioral repertoire. Zebrafish models and tests are particularly useful in CNS drug screening, as well as in modeling complex neurological and psychiatric disorders [71]. The zebrafish genome also shares 70% homology with the human genome, which is valuable for translational medicine, drug discovery, and large-scale chemical screens [72]. Benzo[d]imidazo[2,1-b]thiazoles **11–42** were tested for behavioral activity *in vivo* in order to perform structure–activity relationship analysis. The mostly used "novel tank" test was applied to assess behavioral stress and anxiety indices [47]. Anxiolytic drugs, including Diazepam,[73] can modulate zebrafish "novel tank" behaviors tending to increase time spent in top [74]. We observed anxiety-like behavior for compounds **22**, **36**, **37**, and **38** comprising the group **C**, and, what is surprising, for the $GABA_AR$ α1-selective sedative-hypnotic drug Zolpidem (Figure 4). Moreover, the administration of compounds of the group **B**, including **28**, led to a decrease in time spent in top, alike sedative agents [75]. This results can be attributed to difficulties in distinguishing between anxiety-like and stress-like behavior of zebrafish. Moreover, little is known about $GABA_AR$ diversity and expression in the CNS of zebrafish. Recently, it was shown that zebrafish contain orthologs for most of the $GABA_AR$ subunits found in mammals, but the diversity of subfamilies is bigger [76]. The ability to interact with differently composed $GABA_ARs$, including those specific only for zebrafish, may be responsible for the differences in the observed the drug-induced behavioral effects.

Compounds **28** and **37** were found to be the most active in the series under study and were chosen for detailed biological studies. The observed reduction of the behavioral effects of lead compounds **28** and **37** by after-treatment with Flumazenil suggests the involvement of the α1-containing $GABA_AR$ in drug-induced behavioral responses in zebrafish. The ability of lead compounds **28** and **37** to modulate activity of α1-containing $GABA_AR$ subtypes was tested using electrophysiological experiments in rat cerebellar Purkinje cells, which express the $\alpha1\beta2/3\gamma2$ type of $GABA_AR$ [54]. We found that, as with traditional BZDs, the compounds under study work by enhancing GABAergic inhibitory drive. The molecular modeling confirmed that molecules **28** and **37** interact with the $GABA_AR$ BZD binding site. The different character of interactions of the tested molecules with the BZD binding pocket in the up-right (**37**) and up-left (**28**) modes may also finally result in diverse intrinsic activity evaluated by GABA current measurements and specific features of behavioural effects caused by these drugs. This suggestion is indirectly supported by the finding that even minor transformations (methyl substitution in a single aromatic ring) of 4MP-TQS, which is an nAChR allosteric agonist, resulted in dramatic changes in the ligand action. Derivatives of this ligand exhibit different pharmacological effects on α7 nAChR, from positive to negative, and a silent modulation [77].

Thus, the interactions of lead compound **28** and **37** with α1-containing $GABA_AR$ subtypes may endow these compounds with sedative-hypnotic properties. However, it cannot be ruled out that the effects of these compounds, like most BZD site ligands, are mediated by their complex activity at multiple α subunits and the resulting different behavioral effects, including anxiolytic-like, depend on their affinity/efficacy for modulating activity of different $GABA_AR$ isoforms. The full potential of lead compounds and the exploration of a greater variety of compounds along with elucidation of their $GABA_AR$ selectivity must await additional studies.

CONCLUSION

In the present work, we explored the potential of pyridine/1,3-thiazole bioisosteric replacement in imidazopyridine drugs. Three new classes, imidazo[2,1-b]thiazoles, imidazo[2,1-b][1,3,4]thiadiazoles, and benzo[d]imidazo[2,1-b]thiazoles, bearing aromatic and amide substituents were shown to have potency for binding to the $GABA_AR$ BZD binding site at a nanomolar level. A number of benzo[d]imidazo[2,1-b]thiazoles exhibited the affinity for $GABA_ARs$ (IC_{50} = 6 – 12 nM) that is 3 – 7 times higher compared to the reference drug Zolpidem (IC_{50} = 43 nM). Active compounds were safe and non-toxic at the maximum attainable concentrations in water (up to 47 mg/L). Lead compounds potentiate this GABA-induced current in Purkinje cells with the affinity similar to the estimates for the reference drug Zolpidem in these neurons. We demonstrated an *in vivo* biological efficacy of benzo[d]imidazo[2,1-b]thiazole ligands in behavioral assays using zebrafish as experimental animals. To our delight, the data obtained by the radioligand competition displacement assay and the results of the "novel tank" test providing anxiety behavioral responses in zebrafish corroborate each other and, hence, may be considered to be of a predictive value, allowing a preliminary screening of $GABA_AR$ PAMs. Two groups of active compounds inducing "Zolpidem-alike" and "Zolpidem-like" behavioral responses were formed. The hit compounds from each group, namely **28** and **37** proved to act upon the same mechanism as $GABA_AR$ PAMs potentiating neurons. The structural bases for activity of benzo[d]imidazo[2,1-b]thiazoles were proposed using molecular docking studies.

To sum up, 1,3-thiazole bioisosteric replacement in imidazopyridine drugs has a high potential for the development of new effective and selective $GABA_AR$ PAMs. This approach can be efficient for the elaboration of novel hypnotics, anxiolytics, anticonvulsants, and sedatives. Imidazo[2,1-b]thiazoles, imidazo[2,1-b][1,3,4]thiadiazoles, and benzo[d]imidazo[2,1-b]thiazoles constitute new classes of potent $GABA_AR$ PAMs. The further exploration of these series will be aimed at evaluating their activity in mammals and discovering new candidates for the treatment of central nervous system disorders.

EXPERIMENTAL SECTION

Instruments and Materials

NMR spectra were acquired on Bruker Avance 600 and 300 spectrometers at room temperature; the chemical shifts δ were measured in ppm relative to the solvent (^{1}H: $CDCl_3$, δ = 7.27 ppm, DMSO-d_6, δ = 2.50 ppm; ^{13}C: $CDCl_3$, δ = 77.00 ppm, DMSO-d_6, δ = 39.50 ppm). Splitting patterns are designated as follows: s, singlet; d, doublet; t, triplet; q, quartet; m, multiplet; dd, double doublet. The coupling constants (J) are in Hertz. The structures of all compounds were established using 1D NMR (^{1}H, ^{13}C, JMOD) spectroscopy. Infrared spectra were measured on a FT-IR spectrometer in KBr pellets. High-resolution and accurate mass spectra were obtained on Bruker micrOTOF-QTM ESI-TOF (Electrospray Ionization/Time of Flight) and Thermo Scientific* LTQ Orbitrap mass spectrometers. Melting points (mp) were measured on a Boetius capillary melting point apparatus and are uncorrected. Analytical thin-layer chromatography (TLC) was carried out on silica gel plates (silica gel 60 F254 aluminum supported plates); the

Journal Pre-proofs
visualization was accomplished with an UV lamp (365 nm). Column chromatography was performed on silica gel 60 (60-120 mesh, Merck) or neutral aluminum oxide 0.063 – 0.200 mm (70 - 230 mesh ASTM). Parent *N,N*-dipropyl- and *N,N*-dimethylpropiolamides were prepared according to the published procedure [78]. All reactions were carried out using freshly distilled and dry solvents. Purity was determined by HPLC and confirmed by inspection of NMR spectra (^{1}H and ^{13}C NMR). HPLC analysis was performed using Agilent 1260 equipped with autosampler (Agilent Poroshell 120 C18 column (50 mm × 3.0 mm I.D., 2.7 μm); 0.05% TFA in water/acetonitrile gradient; UV detection at 215 and 254 nm) and electrospray ionization. All test compounds were of ≥ 95% purity. None of the test compounds contain substructures associated with pan-assay interfering activities (PAINS) [79] by inspection or by screening for PAINS or aggregators at http://zinc15.docking.org/patterns/home.

Typical experimental procedure for ethers ***1-7, 11-20***. A screw-capped V-shaped vial (2.0 mL) was charged with 2-aminothiazole (0.36 mmol, 1.0 equiv), aldehyde (0.40 mmol, 1.1 equiv), freshly activated 4Å molecular sieves (300 mg) and dry toluene (1.5 mL). The vial was capped with a pressure cap and stored at 120 °C for 14-24 h until complete consumption of 2-aminothiazole (monitored by ^{1}H NMR). The resulting mixture containing imine was cooled to room temperature and the solvent was removed under reduced pressure. Under inert atmosphere, the residue was redissolved in dry toluene (1 mL) and then CuOTf•C_6H_6 (18 mg, 0.036 mmol, 10 mol %), $Cu(OTf)_2$ (13 mg, 0.036 mmol, 10 mol %), alkyne (0.72 mmol, 2 equiv) and 4Å molecular sieves (100 mg) were added. The reaction mixture was additionally stirred in the vial capped with a pressure cap at 120 °C for 2 h. After the completion of the reaction, the mixture was filtered through a plug of neutral aluminum oxide (eluent – EtOAc). The filtrate was concentrated under reduced pressure to give a crude material, which was purified by column chromatography on silica gel (eluent Et_3N:EtOAc/petroleum ether) or neutral aluminum oxide (eluent EtOAc/petroleum ether) to give product.

Methyl 2-(6-(4-chlorophenyl)imidazo[2,1-b]thiazol-5-yl)acetate (**1**) [44]. Yield 66% (73 mg), yellow solid, mp 123−124 °C; R_f = 0.68 (petroleum ether/EtOAc, 1:3). ^{1}H NMR (600 MHz, $CDCl_3$): δ 7.68 (d, *J* = 8.78 Hz, 2H), 7.53 (d, *J* = 4.53 Hz, 1H), 7.43 (d, *J* = 8.78 Hz, 2H), 6.89 (d, *J* = 4.53 Hz, 1H), 3.94 (s, 2H), 3.79 (s, 3H). ^{13}C NMR (150 MHz, $CDCl_3$) δ 169.7 (CO), 149.3 (C), 144.4 (C), 133.5 (C), 132.6 (C), 129.0 (2×CH), 128.7 (2×CH), 117.9 (CH), 114.4 (C), 112.8 (CH), 52.7 (CH_2), 31.4 (CH_3).

Methyl 2-(6-(4-nitrophenyl)imidazo[2,1-b]thiazol-5-yl)acetate (**2**) [44]. Yield 56% (64 mg), yellow solid, mp 194−195 °C; R_f = 0.54 (hexane/EtOAc, 1:2). ^{1}H NMR (600 MHz, $CDCl_3$) δ 8.35 (d, *J* = 8.73 Hz, 2H), 7.97 (d, *J* = 8.73 Hz, 2H), 7.64 (d, *J* = 4.51 Hz, 1H), 7.08 (d, *J* = 4.51 Hz, 1H), 4.03 (s, 2H), 3.83 (s, 3H). ^{13}C NMR (150 MHz, $CDCl_3$) δ 168.9 (CO), 149.6 (C), 147.2 (C), 141.5 (C), 139.0 (C), 128.3 (2×CH), 124.2 (2×CH), 118.1 (CH), 116.3 (CH), 114.8 (C), 53.0 (CH_2), 31.4 (CH_3).

Ethyl 2-(6-(4-chlorophenyl)imidazo[2,1-b]thiazol-5-yl)acetate (**3**) [44]. Yield 46% (53 mg), yellow solid, mp 111−112 °C; R_f = 0.22 (petroleum ether - EtOAc, 4:1). ^{1}H NMR (300 MHz, $CDCl_3$): δ 7.70 (d, *J* = 8.81 Hz, 2H), 7.53 (d, *J* = 4.41 Hz, 1H), 7.44 (d, *J* = 8.81 Hz, 2H), 6.89 (d, *J* = 4.41 Hz, 1H), 4.23 (q, *J* = 7.33 Hz, 2H), 3.91 (s, 2H), 1.30 (t, *J* = 7.33 Hz, 3H). ^{13}C NMR

Journal Pre-proofs
(75 MHz, $CDCl_3$): δ 169.3 (CO), 149.2 (C), 144.4 (C), 133.3 (C), 132.9 (C), 129.0 (2×CH), 128.9 (2×CH), 117.9 (CH), 114.5 (C), 112.6 (CH), 61.7 (CH_2), 31.6 (CH_2), 14.3 (CH_3).

Ethyl 2-(6-(2,4-dichlorophenyl)imidazo[2,1-b]thiazol-5-yl)acetate (**4**) [44]. Yield 60% (76 mg), yellow solid, mp 80−82 °C; R_f = 0.22 (petroleum ether - EtOAc, 4:1). ^{1}H NMR (300 MHz, $CDCl_3$): δ 7.49−7.50 (m, 3H), 7.32 (dd, *J* = 2.20, 8.76 Hz, 1H), 6.88 (d, *J* = 4.40 Hz, 1H), 4.17 (q, *J* = 7.37 Hz, 2H), 3.76 (s, 2H), 1.25 (t, *J* = 7.37 Hz, 3H). ^{13}C NMR (75 MHz, $CDCl_3$): δ 169.1 (CO), 149.2 (C), 141.7 (C), 134.6 (C), 134.3 (C), 133.4 (CH), 131.7 (C), 129.7 (CH), 127.2 (CH), 118.2 (CH), 116.7 (C), 112.7 (CH), 61.5 (CH_2), 31.3 (CH_2), 14.1 (CH_3).

2-(6-(4-Chlorophenyl)imidazo[2,1-b]thiazol-5-yl)-N,N-dimethylacetamide (**5**)**.** Yield 46% (53 mg), yellow solid, mp 136-138 °C; R_f = 0.33 (petroleum ether - EtOAc, 1:1). ^{1}H NMR (300 MHz, $CDCl_3$): δ 7.63 (d, *J* = 4.70 Hz, 1H), 7.54 (d, *J* = 8.61 Hz, 2H), 7.39 (d, *J* = 8.61 Hz, 2H), 6.79 (d, *J* = 4.70 Hz, 1H), 4.00 (s, 2H), 2.92 (s, 3H), 2.83 (s, 3H). ^{13}C NMR (75 MHz, $CDCl_3$): δ 168.1 (CO), 149.4 (C), 143.2 (C), 133.6 (C), 131.9 (C), 129.2 (2×CH), 128.9 (2×CH), 119.1 (CH), 114.1 (C), 112.5 (CH), 61.2 (CH_2), 36.6 (CH_3), 36.1 (CH_3). IR (KBr) 3433 (w), 2980 (s), 1721 (s), 1582 (s), 1498 (s), 1198 (s), 1014 (s), 739 (w) cm^{-1}. HRMS (ESI/Q-TOF) 320.0606, calcd. for $C_{15}H_{15}ClN_3OS^+$ 320.0619.

Ethyl 2-(6-(4-chlorophenyl)-2-ethylimidazo[2,1-b][1,3,4]thiadiazol-5-yl)acetate (**6**) [44]. Yield 55% (69 mg), yellow solid, mp 125−127 °C; R_f = 0.32 (petroleum ether - EtOAc, 4:1). ^{1}H NMR (300 MHz, $CDCl_3$): δ 7.62 (d, *J* = 8.24 Hz, 2H), 7.38 (d, *J* = 8.24 Hz, 2H), 4.20 (q, *J* = 7.32 Hz, 2H), 4.03 (s, 2H), 3.02 (q, *J* = 7.33 Hz, 2H), 1.41 (t, *J* = 7.32 Hz, 3H), 1.24 (t, *J* = 7.33 Hz, 3H). ^{13}C NMR (75 MHz, $CDCl_3$): δ 169.3 (CO), 153.9 (C), 142.5 (C), 133.2 (C), 132.9 (C), 128.7 (2×CH), 128.4 (2×CH), 116.3 (C), 106.7 (C), 61.4 (CH_2), 30.7 (CH_2), 25.7 (CH_2), 14.1 (CH_3), 13.1 (CH_3).

Ethyl 2-(6-(4-chlorophenyl)-2-isopropylimidazo[2,1-b][1,3,4]thiadiazol-5-yl)acetate (**7**) [44]. Yield 41% (54 mg), yellow solid, mp 137−138 °C; R_f = 0.32 (petroleum ether - EtOAc, 5:1). ^{1}H NMR (300 MHz, $CDCl_3$): δ 7.65 (d, *J* = 8.20 Hz, 2H), 7.40 (d, *J* = 8.20 Hz, 2H), 4.22 (q, *J* = 7.24 Hz, 2H), 4.06 (s, 2H), 3.29− 3.38 (m, 1H), 1.46 (s, 3H), 1.44 (s, 3H), 1.25 (t, *J* = 7.24 Hz, 3H). ^{13}C NMR (75 MHz, $CDCl_3$): δ 170.9 (CO), 169.4 (C), 144.0 (C), 142.4 (C), 133.3 (C), 133.0 (C), 128.8 (2×CH), 128.5 (2×CH), 116.3 (CH), 61.5 (CH_2), 32.5 (CH), 30.8 (CH_2), 22.3 (2×CH_3), 14.2 (CH_3).

Ethyl 2-(6-(4-chlorophenyl)-2-(methoxymethyl)imidazo[2,1-b][1,3,4]thiadiazol-5-yl)acetate (**8**) [44]. Yield 35% (46 mg), yellow solid, mp 109−112 °C; R_f = 0.20 (petroleum ether - EtOAc, 5:1). ^{1}H NMR (300 MHz, $CDCl_3$): δ 7.65 (d, *J* = 8.75 Hz, 2H), 7.41 (d, *J* = 8.75 Hz, 2H), 4.75 (s, 2H), 4.22 (q, *J* = 7.28 Hz, 2H), 4.06 (s, 2H), 3.51 (s, 3H), 1.27 (t, *J* = 7.28 Hz, 3H). ^{13}C NMR (75 MHz, $CDCl_3$): δ 169.1 (CO), 162.8 (C), 144.4 (C), 142.8 (C), 133.5 (C), 132.8 (C), 128.8 (2×CH), 128.6 (2×CH), 116.4 (C), 69.4 (CH_2), 61.6 (CH_2), 59.2 (CH_3), 30.6 (CH_2), 14.1 (CH_3).

2-(6-(4-chlorophenyl)-2-ethylimidazo[2,1-b][1,3,4]thiadiazol-5-yl)-N,N-dimethylacetamide (**9**)**.** Yield 50% (63 mg), yellow solid, mp 140-142 °C; R_f = 0.32 (petroleum ether - EtOAc, 1:1). ^{1}H NMR (300 MHz, $CDCl_3$): δ 7.65 (d, *J* = 8.47 Hz, 2H), 7.37 (d, *J* = 8.47 Hz, 2H), 4.03 (s, 2H),

Journal Pre-proofs
3.16 (s, 3H), 2.99-3.03 (m, 5H), 1.40 (t, J = 7.70 Hz, 3H). ^{13}C NMR (75 MHz, $CDCl_3$): δ 168.3 (CO), 165.9 (C), 143.7 (C), 142.5 (C), 133.2 (C), 133.1 (C), 128.7 (2×CH), 128.6 (2×CH), 117.6 (C), 37.6 (CH_3), 36.0 (CH_3), 29.6 (CH_2), 25.8 (CH_2), 13.1 (CH_3). IR (KBr) 3436 (s), 2918 (s), 1643 (s), 1492 (s), 1396 (s), 1155 (s), 1139 (s), 840 (s) cm^{-1}. HRMS (ESI/Q-TOF) 371.0705, calcd. for $C_{16}H_{17}ClN_4OSNa^+$ 371.0704.

2-(6-(4-chlorophenyl)-2-ethylimidazo[2,1-b][1,3,4]thiadiazol-5-yl)-N,N-dipropylacetamide (**10**)**.** Yield 55% (80 mg), yellow solid, mp 89-90 °C; R_f = 0.32 (petroleum ether - EtOAc, 1:1). ^{1}H NMR (300 MHz, $CDCl_3$): δ 7.67 (d, J = 8.46 Hz, 2H), 7.39 (d, J = 8.46 Hz, 2H), 4.05 (s, 2H), 3.37 (t, J = 7.41 Hz, 4H), 3.02 (q, J = 7.23 Hz, 2H), 1.58-1.72 (m, 4H), 1.42 (t, J = 7.23 Hz, 3H), 0.89-0.99 (m, 6H). ^{13}C NMR (75 MHz, $CDCl_3$): δ 168.1 (CO), 165.8 (C), 143.7 (C), 142.5 (C), 133.3 (C), 133.1 (C), 128.8 (2×CH), 128.7 (2×CH), 118.1 (C), 50.1 (CH_2), 48.3 (CH_2), 29.7 (CH_2), 25.8 (CH_2), 22.4 (CH_2), 21.1 (CH_2), 13.1 (CH_3), 11.4 (CH_3) 11.3 (CH_3). IR (KBr) 3428 (s), 2936 (s), 1631 (s), 1494 (s), 1235 (s), 1146 (s), 1088 (s), 813 (s) cm^{-1}. HRMS (ESI/Q-TOF) 405.1511, calcd. for $C_{20}H_{26}ClN_4OS^+$ 405.1510.

Ethyl (2-phenylimidazo[2,1-b][1,3]benzothiazol-3-yl)acetate (**11**) [44]. Yield 46% (56 mg), yellow solid, mp 80-82 °C; R_f = 0.20 (petroleum ether - EtOAc, 5:1). ^{1}H NMR (300 MHz, $CDCl_3$): δ 7.70-7.81 (m, 4H), 7.47 (dd, J = 7.64 Hz, 3H), 7.31-7.41 (m, 2H), 4.27 (q, J = 7.12 Hz, 2H), 4.21 (s, 2H), 1.28 (t, J = 7.12 Hz, 3H). ^{13}C NMR (75 MHz, $CDCl_3$): δ 169.9 (CO), 147.6 (C), 146.0 (C), 134.0 (C), 133.2 (C), 130.5 (C), 129.1 (2×CH), 128.7 (2×CH), 127.8 (CH), 126.1 (CH) 124.7 (CH), 124.5 (CH), 117.0 (C), 113.1 (CH), 61.8 (CH_2), 31.8 (CH_2), 14.2 (CH_3).

Ethyl [2-(4-methylphenyl)imidazo[2,1-b][1,3]benzothiazol-3-yl]acetate (**12**) [44]. Yield 52% (66 mg), yellow solid, mp 74-77 °C; R_f = 0.23 (petroleum ether - EtOAc, 4:1). ^{1}H NMR (300 MHz, $CDCl_3$): δ 7.80 (d, J = 8.05 Hz, 1H), 7.79 (d, J = 7.53 Hz, 1H), 7.86 (d, J = 8.05 Hz, 2H), 7.43 (dd, J = 7.53 Hz, 1H), 7.36 (dd, J = 8.05 Hz, 1H), 7.29 (d, J = 8.05 Hz, 2H), 4.28 (q, J = 7.29 Hz, 2H), 4.21 (s, 2H), 2.42 (s, 3H), 1.29 (s, J = 7.29 Hz, 3H). ^{13}C NMR (75 MHz, $CDCl_3$): δ 170.0 (CO), 147.5 (C), 146.2 (C), 137.5 (C), 133.2 (C), 131.1 (C), 130.5 (C), 129.4 (2×CH), 128.0 (2×CH), 126.0 (CH), 124.5 (CH), 124.4 (CH), 116.7 (C), 113.0 (CH), 62.0 (CH_2), 31.9 (CH_2), 21.3 (CH_3), 14.2 (CH_3).

Ethyl [2-(4-methoxyphenyl)imidazo[2,1-b][1,3]benzothiazol-3-yl]acetate (**13**) [44]. Yield 45% (59 mg), yellow solid, mp 90-92 °C; R_f = 0.32 (petroleum ether - EtOAc, 4:1). ^{1}H NMR (300 MHz, $CDCl_3$): δ 7.83 (d, J = 8.25 Hz, 1H), 7.75 (d, J = 8.25 Hz, 1H), 7.69 (d, J = 8.24 Hz, 2H), 7.46 (dd, J = 7.33, 8.24 Hz, 1H), 7.27 (dd, J = 7.33, 8.24 Hz, 1H), 7.02 (d, J = 8.24 Hz, 2H), 4.28 (q, J = 7.32 Hz , 2H), 4.19 (s, 2H), 3.87 (s, 3H), 1.28 (t, J = 7.32 Hz, 3H). ^{13}C NMR (75 MHz, $CDCl_3$): δ 169.9 (CO), 159.6 (C), 134.9 (C), 133.1 (C), 132.4 (C), 130.5 (C), 129.5 (2×CH), 126.3 (CH), 125.6 (C), 124.9 (CH), 124.6 (CH), 116.4 (C), 114.3 (2×CH), 113.1 (CH), 61.9 (CH_2), 55.4 (OCH_3), 31.9 (CH_2), 14.3 (CH_3).

Ethyl [2-(2-methoxyphenyl)imidazo[2,1-b][1,3]benzothiazol-3-yl]acetate (**14**) [44]. Yield 42% (55 mg), yellow solid, mp 175-177 °C; R_f = 0.34 (petroleum ether - EtOAc, 4:1). ^{1}H NMR (300 MHz, $CDCl_3$): δ 7.70 (d, J = 8.49 Hz, 1H), 7.62 (d, J = 8.49 Hz, 2H), 7.28-7.42 (m, 3H), 7.07 (dd, J = 7.36 Hz, 1H), 7.00 (d, J = 8.49 Hz, 1H), 4.20 (q, J = 7.32 Hz, 2H), 4.04 (s, 2H), 3.79 (s,

Journal Pre-proofs
3H), 1.22 (t, *J* = 7.32 Hz, 3H). ^{13}C NMR (75 MHz, $CDCl_3$): δ 170.1 (CO), 156.5 (C), 147.3 (C), 142.2 (C), 133.2 (C), 132.0 (CH), 130.5 (C), 129.5 (CH), 126.0 (CH), 124.4 (CH), 124.3 (CH), 123.0 (C), 121.0 (CH), 118.8 (C), 113.0 (CH), 111.3 (CH), 61.3 (CH_2), 55.6 (OCH_3), 31.9 (CH_2), 14.2 (CH_3).

Ethyl [2-(2,4-dimethoxyphenyl)imidazo[2,1-b][1,3]benzothiazol-3-yl]acetate (**15**) [44]. Yield 33% (47 mg), yellow solid, mp 88-90 °C; R_f = 0.31 (petroleum ether - EtOAc, 4:1). ^{1}H NMR (300 MHz, $CDCl_3$): δ 7.87 (d, *J* = 8.07 Hz, 1H), 7.75 (d, *J* = 7.34 Hz, 1H), 7.47 (dd, *J* = 7.34 Hz, 1H), 7.30-7.40 (m, 3H), 6.98 (d, *J* = 8.07 Hz, 1H), 4.29 (q, *J* = 7.34 Hz, 2H), 4.22 (s, 2H), 3.99 (s, 3H), 3.95 (s, 3H), 1.29 (t, *J* = 7.34 Hz, 3H). ^{13}C NMR (75 MHz, $CDCl_3$): δ 169.8 (CO), 149.3 (C), 149.2 (C), 147.3 (C), 144.9 (C), 133.0 (C), 130.4 (C), 126.3 (CH), 125.8 (C), 125.0 (CH), 124.9 (CH), 120.4 (CH), 116.5 (C), 113.3 (CH), 111.5 (CH), 111.3 (CH), 61.9 (CH_2), 56.1 (OCH_3), 56.0 (OCH_3), 31.9 (CH_2), 14.2 (CH_3).

Ethyl [2-(1,3-benzodioxol-5-yl)imidazo[2,1-b][1,3]benzothiazol-3-yl]acetate (**16**) [44]. Yield 50% (68 mg), yellow solid, mp 79-81 °C; R_f = 0.32 (petroleum ether - EtOAc, 4:1). ^{1}H NMR (300 MHz, $CDCl_3$): δ 7.80 (d, *J* = 8.07 Hz, 1H), 7.70 (d, *J* = 7.34 Hz, 1H), 7.42 (dd, *J* = 7.34, 8.07 Hz, 1H), 7.33 (dd, *J* = 7.34, 8.07 Hz, 1H), 7.21-7.28 (m, 2H), 6.90 (d, *J* = 8.07 Hz, 1H), 6.01 (s, 2H), 4.28 (q, *J* = 7.33 Hz, 2H), 4.18 (s, 2H), 1.29 (t, *J* = 7.33 Hz, 3H). ^{13}C NMR (75 MHz, $CDCl_3$): δ 169.9 (CO), 147.9 (C), 147.3 (C), 146.0 (C), 133.1 (C), 130.4 (C), 128.1 (C), 126.0 (CH), 124.5 (CH), 124.4 (CH), 121.8 (CH), 116.4 (C), 112.9 (CH), 110.1 (C), 108.7 (CH), 108.5 (CH), 101.2 (CH_2), 61.8 (CH_2), 31.8 (CH_2), 14.2 (CH_3).

Ethyl [2-(4-fluorophenyl)imidazo[2,1-b][1,3]benzothiazol-3-yl]acetate (**17**) [44]. Yield 48% (61 mg), yellow solid, mp 86-87 °C; R_f = 0.22 (petroleum ether - EtOAc, 5:1). ^{1}H NMR (300 MHz, $CDCl_3$): δ 7.68-7.81 (m, 4H), 7.41 (dd, *J* = 7.76 Hz, 1H), 7.32 (dd, *J* = 7.76 Hz, 1H), 7.15 (dd, *J* = 8.52 Hz, 2H), 4.28 (q, *J* = 7.33 Hz, 2H), 4.16 (s, 2H), 1.28 (t, *J* = 7.33 Hz, 3H). ^{13}C NMR (75 MHz, $CDCl_3$): δ 169.8 (CO), 162.5 (d, $J_{C\text{-}F}$ = 247.1 Hz, C), 147.5 (C), 145.2 (C), 133.0 (C), 130.3 (C), 130.1 (d, $J_{C\text{-}F}$ = 3.2 Hz, C), 129.7 (d, $J_{C\text{-}F}$ = 8.0 Hz, 2×CH), 126.1 (CH), 124.6 (CH), 124.4 (CH), 116.7 (C), 115.5 (d, $J_{C\text{-}F}$ = 21.4 Hz, 2×CH), 113.0 (CH), 61.8 (CH_2), 31.7 (CH_2), 14.2 (CH_3).

Ethyl 2-(2-(4-chlorophenyl)benzo[d]imidazo[2,1-b]tiazole-3-yl)acetate (**18**) [44]. Yield 75% (99 mg), yellow solid, mp 100-102 °C; R_f = 0.20 (petroleum ether - EtOAc, 5:1). ^{1}H NMR (300 MHz, $CDCl_3$): δ 7.84 (d, *J* = 8.07 Hz, 1H), 7.71-7.73 (m, 3H), 7.43-7.48 (m, 3H), 7.37 (dd, *J* = 7.33, 8.07 Hz, 1H), 4.29 (q, *J* = 7.33 Hz, 2H), 4.19 (s, 2H), 1.30 (t, *J* = 7.33 Hz, 3H). ^{13}C NMR (75 MHz, $CDCl_3$): δ 169.6 (CO), 147.7 (C), 144.9 (C), 133.7 (C), 133.0 (C), 132.2 (C), 130.4 (C), 129.2 (2×CH), 128.8 (2×CH), 126.1 (CH), 124.8 (CH), 124.4 (CH), 117.1 (C), 113.1 (CH), 61.9 (CH_2), 31.7 (CH_2), 14.2 (CH_3).

2-(2-(4-Bromophenyl)benzo[d]imidazo[2,1-b]thiazol-3-yl)acetamide (**19**)**.** Yield 78% (117 mg), white solid, mp 105-109 °C; R_f = 0.20 (petroleum ether - EtOAc, 5:1). ^{1}H NMR (300 MHz, $CDCl_3$): δ 7.84 (d, *J* = 8.15 Hz, 1H), 7.73 (d, *J* = 8.15 Hz, 1H), 7.67 (d, *J* = 8.11 Hz, 2H), 7.60 (d, *J* = 8.11 Hz, 2H), 7.46 (dd, *J* = 6.67, 8.15 Hz, 1H), 7.37 (dd, *J* = 6.67, 8.15 Hz, 1H), 4.29 (q, *J* = 7.26 Hz, 2H), 4.19 (s, 2H), 1.30 (t, *J* = 7.26 Hz, 3H). ^{13}C NMR (75 MHz, $CDCl_3$): δ 169.7

Journal Pre-proofs
(CO), 147.8 (C), 145.0 (C), 133.1 (C), 132.9 (C), 131.9 (2×CH), 130.6 (C), 129.6 (2×CH), 126.2 (CH), 124.8 (CH), 124.5 (CH), 121.9 (C), 117.2 (C), 113.1 (CH), 62.0 (CH_2), 31.8 (CH_2), 14.2 (CH_3). IR (KBr) 3347 (w), 2361 (s), 2343 (s), 1736 (s), 1498 (s), 1370 (s), 1193 (s), 847 (s), 738 (s) cm^{-1}. HRMS (ESI/Q-TOF) 415.0098, calcd. for $C_{19}H_{16}BrN_2O_2S^+$ 415.0110.

Ethyl [7-chloro-2-(4-chlorophenyl)imidazo[2,1-b][1,3]benzothiazol-3-yl]acetate (**20**) [44]. Yield 40% (58 mg), yellow solid, mp 188-190 °C; R_f = 0.32 (petroleum ether - EtOAc, 5:1). ^{1}H NMR (300 MHz, $CDCl_3$): δ 7.77 (d, *J* = 8.24 Hz, 1H), 7.68-7.70 (m, 3H), 7.40-7.45 (m, 3H), 4.27 (q, *J* = 7.32 Hz, 2H), 4.14 (s, 2H), 1.29 (t, *J* = 7.32 Hz, 3H). ^{13}C NMR (75 MHz, $CDCl_3$): δ 169.5 (CO), 147.5 (C), 145.4 (C), 133.9 (C), 132.2 (C), 131.9 (C), 131.6 (C), 130.4 (CH), 129.2 (2×CH), 128.8 (2×CH), 126.4 (CH), 124.2 (CH), 117.3 (C), 113.9 (CH), 62.0 (CH_2), 31.6 (CH_2), 14.2 (CH_3).

*Typical experimental procedure for amides **21-42***. Potassium hydroxide (67 mg, 1.20 mmol, 2.0 equiv) in ethanol (1 mL) was added to a solution of ethyl 2-benzo[d]imidazo[2,1-b]tiazole-3-yl acetate (0.60 mmol, 1.0 equiv) in ethanol (10 mL). The reaction mixture was stored at rt for 10 min until the complete conversion of starting material (TLC monitoring). Next, the solvent was removed under reduced pressure, residue was dissolved in water (5 mL) and then glacial acetic acid (0.8 mL) was added. Precipitate formed was filtered, dried under reduced pressure at rt, and suspended in CH_2Cl_2 (5 mL). Phosphorus pentachloride (125 mg, 0.60 mmol, 1.0 equiv) was added in portion. Resulting mixture was heated at 40 °C for 40 min and stored at rt overnight. The flow of ammonia gas was passed through reaction mixture over 30 min (for compounds **21**-**35**) or alkyl amine (0.60 mmol, 1.0 equiv) was added in one portion with following stirring at rt for 60 min (for compounds **36**-**42**). The resulting mixture was washed with ice-water (20 mL), and was extracted with CH_2Cl_2 (3×10 mL). Organic layer was dried over Na_2SO_4, and concentrated in vacuo. The crude product was purified by column chromatography using petroleum ether/ethyl acetate or petroleum ether/EtOAc, 1:2 eluent.

2-(2-Phenylbenzo[d]imidazo[2,1-b]thiazol-3-yl)acetamide (**21**)**.** Yield 74% (136 mg), white solid, mp 243-245 °C ($mp_{lit[40]}$ 246-248 °C); R_f = 0.21 (petroleum ether - EtOAc, 1:1). ^{1}H NMR (300 MHz, DMSO-d_6): δ 8.06 (d, *J* = 8.07 Hz, 1H), 7.84-7.87 (m, 2H), 7.68 (d, *J* = 8.07 Hz, 2H), 7.35-7.57 (m, 6H), 4.12 (s, 2H). ^{13}C NMR (75 MHz, DMSO-d_6): δ 170.4 (CO), 146.3 (C), 144.3 (C), 134.1 (C), 132.7 (C), 129.2 (C), 128.5 (2×CH), 127.3 (2×CH), 127.2 (CH), 126.3 (CH), 124.9 (CH), 124.7 (CH), 119.5 (C), 113.5 (CH), 31.7 (CH_2). IR (KBr) 3438 (w), 2365 (s), 2345 (s), 1676 (s), 1497 (s), 1388 (s), 1073 (s), 745 (s), 703 (s) cm^{-1}. HRMS (ESI/Q-TOF) 308.0850, calcd. for $C_{17}H_{14}N_3OS^+$ 308.0852.

2-(2-(p-Tolyl)benzo[d]imidazo[2,1-b]thiazol-3-yl)acetamide (**22**)**.** Yield 65% (125 mg), white solid, mp 252-253 °C ($mp_{lit[40]}$ 253-254 °C); R_f = 0.20 (petroleum ether - EtOAc, 1:1). ^{1}H NMR (300 MHz, DMSO-d_6): δ 8.04 (d, *J* = 8.28 Hz, 1H), 7.82-7.85 (m, 2H), 7.50-7.57 (m, 3H), 7.42 (dd, *J* = 7.21, 8.28 Hz, 1H), 7.34 (br.s, 1H), 7.28 (d, *J* = 8.19 Hz, 2H), 4.09 (s, 2H), 2.36 (s, 3H). ^{13}C NMR (75 MHz, DMSO-d_6): δ 170.6 (CO), 144.5 (C), 136.5 (C), 132.7 (C), 131.4 (C), 129.2 (2×CH), 129.1 (C), 129.0 (C), 127.3 (2×CH), 126.3 (CH), 124.9 (CH), 124.6 (CH), 119.1 (C), 113.4 (CH), 31.8 (CH_2), 20.8 (CH_3). IR (KBr) 3437 (w), 2361 (s), 2342 (s), 1679 (s), 1508 (s),

Journal Pre-proofs
1488 (s), 1388 (s), 1370(s), 1110 (s), 755 (s), cm $^{-1}$. HRMS (ESI/Q-TOF) 322.1013, calcd. for $C_{18}H_{16}N_3OS^+$ 322.1009.

2-(2-(4-Methoxyphenyl)benzo[d]imidazo[2,1-b]thiazol-3-yl)acetamide (**23**)**.** Yield 71% (144 mg), white solid, mp 285-287 °C ($mp_{lit[40]}$ 285-287 °C); R_f = 0.23 (petroleum ether - EtOAc, 1:1). ^{1}H NMR (300 MHz, DMSO-d_6): δ 8.04 (d, *J* = 8.22 Hz, 1H), 7.83-7.85 (m, 2H), 7.60 (d, *J* = 8.82 Hz, 2H), 7.53 (dd, *J* = 7.22, 8.22 Hz, 1H), 7.42 (dd, *J* = 7.22, 8.22 Hz, 1H), 7.32 (br.s, 1H), 7.06 (d, *J* = 8.82 Hz, 2H), 4.08 (s, 2H), 3.82 (s, 3H). ^{13}C NMR (75 MHz, DMSO-d_6): δ 170.6 (CO), 158.6 (C), 145.6 (C), 144.3 (C), 132.7 (C), 129.2 (C), 128.6 (2×CH), 126.7 (C), 126.3 (CH), 124.9 (CH), 124.5 (CH), 118.6 (C), 114.0 (2×CH), 113.3 (CH), 55.1 (CH_3), 31.8 (CH_2). IR (KBr) 3306 (w), 2362 (s), 2343 (s), 1677 (s), 1509 (s), 1374 (s), 1254 (s), 1176 (s), 1038 (s), 830 (s), 739 (s) cm^{-1}. HRMS (ESI/Q-TOF) 338.0945, calcd. for $C_{18}H_{16}N_3O_2S^+$ 338.0958.

2-(2-(2-Methoxyphenyl)benzo[d]imidazo[2,1-b]thiazol-3-yl)acetamide (**24**)**.** Yield 75% (152 mg), white solid, mp 264-265 °C; R_f = 0.23 (petroleum ether - EtOAc, 1:1). ^{1}H NMR (300 MHz, DMSO-d_6): δ 8.01 (d, *J* = 7.74 Hz, 1H), 7.75 (d, *J* = 7.74 Hz, 1H), 7.35-7.50 (m, 4H), 7.09 (d, *J* = 8.05 Hz, 1H), 7.02 (dd, *J* = 6.85, 7.74 Hz, 1H), 4.05 (s, 2H), 3.66 (s, 3H) (the signal of the NH_2 was not observed). ^{13}C NMR (75 MHz, DMSO-d_6): δ 169.9 (CO), 155.4 (C), 132.1 (C), 130.9 (CH), 128.9 (CH), 128.6 (C), 125.9 (CH), 125.8 (C), 124.3 (CH), 124.2 (CH), 122.1 (C), 120.0 (CH), 118.7 (C), 113.3 (C), 113.2 (CH), 111.0 (CH), 55.7 (CH_3), 30.4 (CH_2). IR (KBr) 3372 (w), 2369 (s), 2340 (s), 1669 (s), 1497 (s), 1108 (s), 834 (s), 796 (s) cm^{-1}. HRMS (ESI/Q-TOF) 338.0957, calcd. for $C_{18}H_{16}N_3O_2S^+$ 338.0957.

2-(2-(2,4-Dimethoxyphenyl)benzo[d]imidazo[2,1-b]thiazol-3-yl)acetamide (**25**)**.** Yield 63% (139 mg), white solid, mp 261-263 °C; R_f = 0.25 (petroleum ether - EtOAc, 1:1). ^{1}H NMR (300 MHz, DMSO-d_6): δ 8.03 (d, *J* = 7.33 Hz, 1H), 7.84-7.87 (m, 2H), 7.53 (dd, *J* = 6.61, 8.13 Hz, 1H), 7.42 (dd, *J* = 6.61, 8.13 Hz, 1H), 7.36 (s, 1H), 7.27 (br.s, 1H), 7.18 (d, *J* = 8.13 Hz, 1H), 7.06 (d, *J* = 8.13 Hz, 1H), 4.11 (s, 2H), 3.83 (s, 3H), 3.82 (s, 3H). ^{13}C NMR (75 MHz, DMSO-d_6): δ 170.8 (CO), 148.7 (C), 148.3 (C), 144.5 (C), 132.8 (C), 129.3 (C), 127.0 (C), 126.3 (CH), 124.9 (2×CH), 124.6 (CH), 119.6 (CH), 118.8 (C), 113.5 (CH), 111.9 (CH), 111.3 (C), 55.6 (CH_3), 55.4 (CH_3), 31.9 (CH_2). IR (KBr) 3409 (w), 2389 (s), 2340 (s), 1663 (s), 1494 (s), 1094 (s), 835 (s), 799 (s) cm^{-1}. HRMS (ESI/Q-TOF) 368.1061, calcd. for $C_{19}H_{18}N_3O_3S^+$ 368.1063.

2-(2-(2-Chlorophenyl)benzo[d]imidazo[2,1-b]thiazol-3-yl)acetamide (**26**)**.** Yield 59% (121 mg), white solid, mp 203-205 °C ($mp_{lit[40]}$ 244-246 °C); R_f = 0.28 (petroleum ether - EtOAc, 1:1). ^{1}H NMR (300 MHz, DMSO-d_6): δ 8.06 (d, *J* = 8.06 Hz, 1H), 7.79 (d, *J* = 7.33 Hz, 1H), 7.46-7.65 (m, 7H), 3.87 (s, 2H). ^{13}C NMR (75 MHz, DMSO-d_6): δ 170.2 (CO), 145.7 (C), 142.2 (C), 133.0 (C), 132.7 (C), 132.6 (CH), 132.5 (CH), 129.9 (C), 129.8 (CH), 129.2 (CH), 127.1 (C), 126.3 (CH), 124.92 (2×CH), 121.0 (C), 113.8 (CH), 31.4 (CH_2). IR (KBr) 3442 (w), 1727 (s), 1499 (s), 1376 (s), 1256 (s), 1080 (s), 1035 (s), 828 (s), 743 (s) cm^{-1}. HRMS (ESI/Q-TOF) 342.0462, calcd. for $C_{17}H_{13}ClN_3OS^+$ 342.0452.

2-(2-(3-Chlorophenyl)benzo[d]imidazo[2,1-b]thiazol-3-yl)acetamide (**27**)**.** Yield 78% (160 mg), white solid, mp 243-245 °C ($mp_{lit[40]}$ 242-245 °C); R_f = 0.28 (petroleum ether - EtOAc, 1:1). ^{1}H

Journal Pre-proofs
NMR (600 MHz, DMSO-d_6): δ 8.06 (d, *J* = 7.34 Hz, 1H), 7.87-7.93 (m, 2H), 7.73 (s, 1H), 7.65 (d, *J* = 7.34 Hz, 1H), 7.40-7.58 (m, 5H), 4.15 (s, 2H). ^{13}C NMR (75 MHz, DMSO-d_6): δ 170.3 (CO), 146.3 (C), 142.9 (C), 136.2 (C), 133.4 (C), 132.6 (C), 130.5 (CH), 129.4 (C), 127.1 (CH), 126.9 (CH), 126.4 (CH), 125.7 (CH), 125.0 (2×CH), 120.3 (C), 113.6 (CH), 31.7 (CH_2). IR (KBr) 3440 (s), 1675 (s), 1599 (s), 1493 (s), 1368 (s), 1318 (s), 1078 (s), 1032 (s), 755 (s) cm^{-1}. HRMS (ESI/Q-TOF) 342.0461, calcd. for $C_{17}H_{13}ClN_3OS^+$ 342.0462.

2-(2-(4-Chlorophenyl)benzo[d]imidazo[2,1-b]thiazol-3-yl)acetamide (**28**)**.** Yield 61% (125 mg), white solid, mp 285-287 °C ($mp_{lit[40]}$ 288-290 °C); R_f = 0.27 (petroleum ether - EtOAc, 1:1). ^{1}H NMR (300 MHz, DMSO-d_6): δ 8.03 (d, *J* = 8.15 Hz, 1H), 7.85 (d, *J* = 7.68 Hz, 2H), 7.68 (d, *J* = 7.68 Hz, 2H), 7.51-7.54 (m, 3H), 7.42 (dd, *J* = 6.99, 8.15 Hz, 1H), 7.32 (br.s, 1H), 4.10 (s, 2H). ^{13}C NMR (75 MHz, DMSO-d_6): δ 170.3 (CO), 144.0 (C), 143.7 (C), 133.5 (C), 133.1 (C), 132.3 (C), 129.3 (C), 128.9 (2×CH), 128.6 (2×CH), 126.3 (CH), 124.9 (CH), 124.8 (C), 120.3 (C), 113.5 (CH), 31.7 (CH_2). IR (KBr) 3343 (s), 1668 (s), 1497 (s), 1395 (s), 1092 (s), 835 (s), 743 (s) $см^{-1}$. HRMS (ESI/Q-TOF) 342.0454, calcd. for $C_{17}H_{13}ClN_3OS^+$ 342.0462.

2-(7-Chloro-2-(4-chlorophenyl)benzo[d]imidazo[2,1-b]thiazol-3-yl)acetamide (**29**)**.** Yield 56% (126 mg), white solid, mp 240-242 °C; R_f = 0.25 (petroleum ether - EtOAc, 1:1). ^{1}H NMR (300 MHz, DMSO-d_6): δ 8.26 (br.s, 1H), 7.86 (d, *J* = 7.33 Hz, 2H), 7.69 (d, *J* = 7.33 Hz, 2H), 7.59-7.63 (m, 1H), 7.53-7.56 (m, 2H), 7.36 (br.s, 1H), 4.11 (s, 2H). IR (KBr) 3368 (w), 2361 (s), 2343 (s), 1670 (s), 1499 (s), 1296 (s), 1100 (s), 1012 (s), 833 (s), 804 (s) cm^{-1}. HRMS (ESI/Q-TOF) 376.0059, calcd. for $C_{17}H_{12}Cl_2N_3OS^+$ 376.0072.

2-(2-(4-Chlorophenyl)-7-methoxybenzo[d]imidazo[2,1-b]thiazol-3-yl)acetamide (**30**)**.** Yield 47% (105 mg), white solid, mp 275-278 °C; R_f = 0.20 (petroleum ether - EtOAc, 1:1). ^{1}H NMR (300 MHz, DMSO-d_6): δ 7.92 (br.s, 1H), 7.79 (d, *J* = 8.79 Hz, 1H), 7.70 (m, 3H), 7.52 (d, *J* = 8.79 Hz, 2H), 7.29 (br.s, 1H), 7.10 (dd, *J* = 2.47, 8.95 Hz, 1H), 4.09 (s, 2H), 3.85 (s, 3H). ^{13}C NMR (75 MHz, DMSO-d_6): δ 170.3 (CO), 156.6 (C), 142.6 (C), 133.2 (C), 131.7 (C), 130.7 (C), 128.8 (2×CH), 128.6 (3×CH), 126.7 (C), 119.7 (C), 114.2 (C), 113.4 (CH), 109.4 (CH), 55.8 (CH_3), 31.6 (CH_2). IR (KBr) 3449 (w), 1674 (s), 1501 (s), 1401 (s), 1225 (s), 829 (s), 806 (s) cm^{-1}. HRMS (ESI/Q-TOF) 372.0560, calcd. for $C_{18}H_{15}ClN_3O_2S^+$ 372.0568.

2-(2-(2,4-Dichlorophenyl)benzo[d]imidazo[2,1-b]thiazol-3-yl)acetamide (**31**)**.** Yield 90% (203 mg), white solid, mp 237-239 °C; R_f = 0.27 (petroleum ether - EtOAc, 1:1). ^{1}H NMR (300 MHz, DMSO-d_6): δ 8.05 (d, *J* = 8.24 Hz, 1H), 7.81 (d, *J* = 8.24 Hz, 1H), 7.76 (s, 1H), 7.66 (br.s, 1H), 7.50-7.53 (m, 3H), 7.43 (dd, *J* = 7.43, 8.24 Hz, 1H), 7.20 (br.s, 1H), 3.88 (s, 2H). ^{13}C NMR (75 MHz, DMSO-d_6): δ 170.0 (CO), 145.8 (C), 141.1 (C), 134.0 (C), 133.7 (CH), 133.5 (C), 132.5 (C), 131.8 (C), 129.3 (CH), 129.2 (C), 127.3 (CH), 126.3 (CH), 124.8 (2×CH), 121.4 (C), 113.8 (CH), 31.3 (CH_2). IR (KBr) 3350 (w), 2362 (s), 2344 (s), 1671 (s), 1493 (s), 1389 (s), 1314 (s), 1125 (s), 1028 (s), 830 (s), 744 (s) cm^{-1}. HRMS (ESI/Q-TOF) 376.0055, calcd. for $C_{17}H_{12}Cl_2N_3OS^+$ 376.0072.

2-(2-(3,4-Dichlorophenyl)benzo[d]imidazo[2,1-b]thiazol-3-yl)acetamide (**32**)**.** Yield 68% (153 mg), white solid, mp 230-232 °C; R_f = 0.27 (petroleum ether - EtOAc, 1:1). ^{1}H NMR (300 MHz, DMSO-d_6): δ 8.07 (d, *J* = 7.33 Hz, 1H), 7.90-7.92 (m, 3H), 7.75 (d, *J* = 8.06 Hz, 1H), 7.67 (d, *J*

Journal Pre-proofs
= 8.06 Hz, 1H), 7.56 (dd, *J* = 7.33 Hz, 1H), 7.46 (dd, *J* = 7.33 Hz, 1H), 7.39 (s, 1H), 4.15 (s, 2H). IR (KBr) 3433 (w), 1727 (s), 1495 (s), 1366 (s), 1254 (s), 1088 (s), 1030 (s), 828 (s), 743 (s) cm^{-1}. HRMS (ESI/Q-TOF) 376.0006, calcd. for $C_{17}H_{12}Cl_2N_3OS^+$ 376.0072.

2-(2-(4-Fluorophenyl)benzo[d]imidazo[2,1-b]thiazol-3-yl)acetamide (**33**)**.** Yield 84% (163 mg), white solid, mp 266-268 °C ($mp_{lit[40]}$ 268-270 °C); R_f = 0.21 (petroleum ether - EtOAc, 1:1). ^1H NMR (300 MHz, DMSO-d_6): δ 8.05 (d, *J* = 7.33 Hz, 1H), 7.87 (d, *J* = 8.79 Hz, 2H), 7.71 (dd, *J* = 5.60, 8.79 Hz, 2H), 7.54 (dd, *J* = 6.58, 7.33 Hz, 1H), 7.43 (dd, *J* = 6.58, 7.33 Hz, 1H), 7.29-7.35 (m, 3H), 4.10 (s, 2H). ^{13}C NMR (75 MHz, $CDCl_3$): δ 170.4 (CO), 162.0 (d, J_{C-F} = 244.0 Hz, C), 146.3 (C), 144.0 (C), 133.1 (C), 131.1 (d, J_{C-F} = 3.0 Hz, C), 129.9 (C), 129.8 (d, J_{C-F} = 8.1 Hz, 2×CH), 126.1 (CH), 125.5 (CH), 125.2 (CH), 119.9 (C), 115.5 (d, J_{C-F} = 21.4 Hz, 2×CH), 113.9 (CH), 31.1 (CH_2). IR (KBr) 3347 (w), 3149 (s), 2375 (s), 2345 (s), 1668 (s), 1508 (s), 1489 (s), 1396 (s), 1225 (s), 1158 (s), 839 (s), 744 (s) cm^{-1}. HRMS (ESI/Q-TOF) 326.0749, calcd. for $C_{17}H_{13}FN_3OS^+$ 326.0758.

2-(2-(4-Bromophenyl)benzo[d]imidazo[2,1-b]thiazol-3-yl)acetamide (**34**)**.** Yield 76% (176 mg), white solid, mp 214-216 °C ($mp_{lit[41]}$ 214-215 °C); R_f = 0.23 (petroleum ether - EtOAc, 1:1). ^1H NMR (300 MHz, DMSO-d_6): δ 8.05 (d, *J* = 7.67 Hz, 1H), 7.92 (br.s, 1H), 7.88 (d, *J* = 7.67 Hz, 1H), 7.62-7.69 (m, 4H), 7.54 (dd, *J* = 7.67 Hz, 1H), 7.44 (dd, *J* = 7.67 Hz, 1H), 7.35 (br.s, 1H), 4.12 (s, 2H). ^{13}C NMR (75 MHz, DMSO-d_6): δ 170.3 (CO), 152.3 (C), 152.2 (C), 143.2 (C), 133.4 (C), 132.6 (C), 131.5 (2×CH), 129.2 (2×CH), 126.4 (CH), 124.9 (CH), 124.8 (CH), 120.4 (C), 120.0 (C), 113.6 (CH), 31.7 (CH_2). IR (KBr) 3360 (w), 3152 (w), 2388 (s), 2347 (s), 1666 (s), 1498 (s), 1397 (s), 1071 (s), 831 (s), 743 (s) cm^{-1}. HRMS (ESI/Q-TOF) 387.9931, calcd. for $C_{17}H_{13}BrN_3OS^+$ 387.9937.

2-(2-(4-(Trifluoromethyl)phenyl)benzo[d]imidazo[2,1-b]thiazol-3-yl)acetamide (**35**)**.** Yield 81% (182 mg), white solid, mp 229-230 °C; R_f = 0.20 (petroleum ether - EtOAc, 1:1). ^1H NMR (300 MHz, DMSO-d_6): δ 8.07 (d, *J* = 7.33 Hz, 1H), 7.86-7.95 (m, 4H), 7.84 (d, *J* = 8.79 Hz, 2H), 7.56 (dd, *J* = 7.33 Hz, 1H), 7.46 (dd, *J* = 7.33 Hz, 1H), 7.39 (br.s, 1H), 4.18 (s, 2H). ^{13}C NMR (75 MHz, DMSO-d_6): δ 170.2 (CO), 146.5 (C), 142.8 (C), 138.2 (C), 132.5 (C), 129.4 (C), 127.7 (2×CH), 127.5 (q, J_{C-F} = 33.1 Hz, C), 127.1 (CH), 125.5 (CH), 125.5 (CH), 125.0 (2×CH), 122.5 (q, J_{C-F} = 395.0 Hz, CF_3), 121.0 (C), 113.7 (CH), 31.7 (CH_2). IR (KBr) 3350 (w), 2363 (s), 2344 (s), 1670 (s), 1496 (s), 1330 (s), 1167 (s), 1112 (s), 1068 (s), 743 (s) cm^{-1}. HRMS (ESI/Q-TOF) 376.0718, calcd. for $C_{18}H_{13}F_3N_3OS^+$ 376.0726.

N,N-Dimethyl-2-(2-(p-tolyl)benzo[d]imidazo[2,1-b]thiazol-3-yl)acetamide (**36**)**.** Yield 32% (42 mg), yellow solid, mp 234-236 °C ($mp_{lit[40]}$ 238-239 °C); R_f = 0.20 (petroleum ether - EtOAc, 1:1). ^1H NMR (300 MHz, $CDCl_3$): δ 7.66 (d, *J* = 7.84 Hz, 1H), 7.61 (d, *J* = 7.84 Hz, 1H), 7.50 (d, *J* = 8.07 Hz, 2H), 7.38 (dd, *J* = 7.84 Hz, 1H), 7.24-7.31 (m, 3H), 4.19 (s, 2H), 3.10 (s, 3H), 3.05 (s, 3H), 2.40 (s, 3H). ^{13}C NMR (75 MHz, $CDCl_3$): δ 168.8 (CO), 147.3 (C), 145.7 (C), 137.2 (C), 133.3 (C), 131.5 (C), 130.3 (C), 129.3 (2×CH), 128.0 (2×CH), 126.0 (CH), 124.3 (CH), 124.1 (CH), 118.0 (C), 113.2 (CH), 37.5 (CH_3), 36.1 (CH_3), 30.9 (CH_2), 21.3 (CH_3). IR (KBr) 3424 (s), 2925 (s), 1645 (s), 1509 (s), 1487 (s), 1394 (s), 1138 (s), 824 (s), 743 (s) cm^{-1}. HRMS (ESI/Q-TOF) 350.1314, calcd. for $C_{20}H_{20}N_3OS^+$ 350.1322.

Journal Pre-proofs

2-(2-(2-Chlorophenyl)benzo[d]imidazo[2,1-b]thiazol-3-yl)-N,N-dimethylacetamide (**37**)**.** Yield 30% (40 mg), yellow solid, mp 154-156 °C (mp_{lit}[40] 159-162 °C); R_f = 0.32 (petroleum ether - EtOAc, 1:1). ^{1}H NMR (300 MHz, $CDCl_3$): δ 7.74 (d, *J* = 8.07 Hz, 1H), 7.68 (d, *J* = 8.07 Hz, 1H), 7.52-7.54 (m, 1H), 7.49-7.50 (m, 1H), 7.40 (dd, *J* = 7.36, 8.44 Hz, 1H), 7.30-7.34 (m, 3H), 4.04 (s, 2H), 2.98 (s, 3H), 2.96 (s, 3H). ^{13}C NMR (75 MHz, $CDCl_3$): δ 168.5 (CO), 147.5 (C), 142.8 (C), 133.8 (C), 133.4 (C), 133.2 (C), 132.9 (CH), 130.4 (C), 129.9 (CH), 129.5 (CH), 126.9 (CH), 126.0 (CH), 124.5 (CH), 124.1 (CH), 120.0 (C), 113.8 (CH), 37.4 (CH_3), 36.0 (CH_3), 30.9 (CH_2). IR (KBr) 3432 (s), 3054 (s), 2927 (s), 1644 (s), 1491 (s), 1396 (s), 1313 (s), 1140 (s), 1037 (s), 760 (s) cm^{-1}. HRMS (ESI/Q-TOF) 370.0762 calcd. for $C_{19}H_{17}ClN_3OS^+$ 370.0775.

2-(2-(3-Chlorophenyl)benzo[d]imidazo[2,1-b]thiazol-3-yl)-N,N-dimethylacetamide (**38**)**.** Yield 30% (40 mg), yellow solid, mp 151-152 °C ($mp_{lit[40]}$ 156 °C); R_f = 0.32 (petroleum ether - EtOAc, 1:1). ^{1}H NMR (300 MHz, $CDCl_3$): δ 7.67 (d, *J* = 7.89 Hz, 1H), 7.58-7.60 (m, 2H), 7.48 (dd, *J* = 7.64, 9.20 Hz, 1H), 7.29-7.39 (m, 4H), 4.19 (s, 2H), 3.10 (s, 3H), 3.07 (s, 3H). ^{13}C NMR (75 MHz, $CDCl_3$): δ 168.4 (CO), 147.7 (C), 144.2 (C), 136.2 (C), 134.5 (C), 133.2 (C), 130.5 (C), 129.9 (CH), 128.0 (CH), 127.5 (CH), 126.1 (2×CH), 124.6 (CH), 124.3 (CH), 118.9 (C), 113.3 (CH), 37.5 (CH_3), 36.1 (CH_3), 30.7 (CH_2). IR (KBr) 3431 (w), 2921 (s), 1645 (s), 1495 (s), 1396 (s), 1140 (s, 795 (s), 747 (s), 713 (s) cm^{-1}. HRMS (ESI/Q-TOF) 370.0764, calcd. for $C_{19}H_{17}ClN_3OS^+$ 370.0775.

2-[2-(4-Chlorophenyl)imidazo[2,1-b][1,3]benzothiazol-3-yl]-N,N-dimethylacetamide (**39**) [44]. Yield 61% (81 mg), yellow solid, mp 234-236 °C; R_f = 0.32 (petroleum ether - EtOAc, 1:1). ^{1}H NMR (300 MHz, $CDCl_3$): δ 7.68 (d, *J* = 8.12 Hz, 1H), 7.53-7.58 (m, 3H), 7.37-7.42 (m, 3H), 7.31 (dd, *J* = 7.33, 8.12 Hz, 1H), 4.17 (s, 2H), 3.15 (s, 3H), 3.07 (s, 3H). ^{13}C NMR (75 MHz, $CDCl_3$): δ 168.4 (CO), 147.6 (C), 144.5 (C), 133.4 (C), 133.1 (C), 132.8 (C), 130.5 (C), 129.4 (2×CH), 128.8 (2×CH), 126.1 (CH), 124.6 (CH), 124.3 (CH), 118.5 (C), 113.1 (CH), 37.5 (CH_3), 36.1 (CH_3), 30.8 (CH_2).

2-(2-(2,4-Dichlorophenyl)benzo[d]imidazo[2,1-b]thiazol-3-yl)-N,N-dimethylacetamide (**40**)**.** Yield 30% (72 mg), yellow solid, mp 147-146 °C; R_f = 0.35 (petroleum ether - EtOAc, 1:1). ^{1}H NMR (300 MHz, $CDCl_3$): δ 7.64-7.70 (m, 2H), 7.52 (d, *J* = 2.01 Hz, 1H), 7.47 (d, *J* = 8.24 Hz, 1H), 7.39 (dd, *J* = 7.36, 8.24 Hz, 1H), 7.31-7.34 (m, 2H), 4.01 (s, 2H), 3.03 (s, 3H), 2.97 (s, 3H). ^{13}C NMR (75 MHz, $CDCl_3$): δ 168.3 (CO), 147.7 (C), 141.8 (C), 134.7 (C), 134.5 (C), 133.77 (CH), 133.3 (C), 131.9 (C), 130.5 (C), 129.7 (CH), 127.3 (CH), 126.1 (CH), 124.7 (CH), 124.2 (CH), 120.2 (C), 113.7 (CH), 37.5 (CH_3), 36.0 (CH_3), 30.9 (CH_2). IR (KBr) 3432 (s), 2923 (w), 1650 (s), 1493 (s), 1393 (s), 1127 (s), 824 (s), 744 (s), 727 (c) cm^{-1}. HRMS (ESI/Q-TOF) 404.0377, calcd. for $C_{19}H_{16}Cl_2N_3OS^+$ 404.0386.

2-(2-(4-Chlorophenyl)benzo[d]imidazo[2,1-b]thiazol-3-yl)-N,N-diethylacetamide (**41**)**.** Yield 95% (226 mg), yellow solid, mp 229-231 °C; R_f = 0.28 (petroleum ether - EtOAc, 1:1). ^{1}H NMR (300 MHz, $CDCl_3$): δ 7.64 (d, *J* = 7.33 Hz, 1H), 7.54 (d, *J* = 7.33 Hz, 1H), 7.52 (d, *J* = 8.07 Hz, 2H), 7.38 (d, *J* = 8.07 Hz, 2H), 7.24-7.34 (m, 2H), 4.12 (s, 2H), 3.37-3.48 (m, 4H), 1.12-1.23 (m, 6H). ^{13}C NMR (75 MHz, $CDCl_3$): δ 167.4 (CO), 147.3 (C), 144.2 (C), 133.1 (C), 132.9 (C), 132.8 (C), 130.2 (C), 129.1 (2×CH), 128.6 (2×CH), 125.8 (CH), 124.4 (CH), 124.1 (CH), 118.7

Journal Pre-proofs
(C), 113.1 (CH), 42.3 (CH_2), 40.8 (CH_2), 30.7 (CH_2), 14.3 (CH_3), 13.4 (CH_3). IR (KBr) 3426 (w), 2976 (w), 1634 (s), 1498 (s), 1460 (w), 841 (w), 748 (w) cm^{-1}. HRMS (ESI/Q-TOF) 398.1080, calcd. for $C_{21}H_{21}ClN_3OS^+$ 398.1088.

2-[2-(4-Chlorophenyl)imidazo[2,1-b][1,3]benzothiazol-3-yl]-N,N-dipropylacetamide (**42**) [44]. Yield 75% (191 mg), yellow solid, mp 85-87 °C; R_f = 0.32 (petroleum ether - EtOAc, 4:1). ^{1}H NMR (300 MHz, $CDCl_3$): δ 7.67 (d, *J* = 7.34 Hz, 1H), 7.55 (d, *J* = 8.07 Hz, 1H), 7.54 (d, *J* = 8.07 Hz, 2H), 7.40 (d, *J* = 8.07 Hz, 2H), 7.37 (dd, *J* = 8.07 Hz, 1H), 7.29 (dd, *J* = 7.34, 8.07 Hz, 1H), 4.17 (s, 2H), 3.32-3.42 (m, 4H), 1.57-1.71 (m, 4H), 0.90-0.98 (m, 6H). ^{13}C NMR (75 MHz, $CDCl_3$): δ 168.0 (CO), 147.5 (C), 144.5 (C), 133.4 (C), 133.2 (C), 133.0 (C), 130.4 (C), 129.3 (2×CH), 128.7 (2×CH), 125.9 (CH), 124.5 (CH), 124.3 (CH), 118.8 (C), 113.1 (CH), 49.9 (CH_2), 48.1 (CH_2), 30.9 (CH_2), 22.3 (CH_2), 21.0 (CH_2), 11.4 (CH_3), 11.3 (CH_3).

Radioligand displacement assays

Membrane Preparation. Fresh brain tissue of several species was homogenized in 16 mL of ice-cold (0–4°C) 50 mM TRIS-HCl buffer (pH 7.4) with a Potter S homogenizer (Sartorius). The homogenate was centrifuged at 42000 g for 25 min in an Optima L-70K centrifuge (Beckman Coulter), and the resulting supernatant was resuspended in 16 mL of ice-cold (0–4°C) 50 mM TRIS-HCl buffer (pH 7.4). The obtained membranes were washed at least three times by re-homogenization in the same amount of ice–cold (0–4°C) 50 mM TRIS-HCl buffer (pH 7.4) and recentrifugation. The final membrane fraction was suspended in 20 mL of TRIS-HCl buffer (pH 7.4) and used in 250 μL portions for each binding experiment.

Replacement Assays. The [^{3}H]Flunitrazepam ([*N*-methyl-^{3}H]Flunitrazepam) binding was determined as described in the study.[30] The standard incubation medium (final volume 0.5 mL) contained membranes (about 250 μg of protein), 3 nM [^{3}H]Flunitrazepam, 67.4 Ci/mmol in 50 mM Tris-HCl buffer (pH 7.4). The compounds to be tested were added at the stated concentrations. At the end of the incubation period (0–4 °C, 30 min), 5 mL of ice-cold buffer (50 mM Tris, pH 7.4) was immediately added, and the membranes with bound [^{3}H]Flunitrazepam were trapped on Whatman GF/B glass fiber filters. The filters were instantly washed with additional 5 mL of the ice-cold buffer and dried in air at room temperature. Nonspecific binding was determined in the same incubation mixture in the presence of excess (20 μM) unlabeled Diazepam and was subtracted from the total binding to yield specific binding. The radioactivity of each sample was measured for 2 min with a Tri-Carb 2900-TR (Perkin Elmer) scintillation counter. The counting efficiency was 45%. The nonspecific binding was no more than 10% of the total binding.

Behavioral effects on adult zebrafish

Animals and housing. Adult mature (5–7 months) male and female wild-type short-fin zebrafish (approximately 50 : 50 male : female ratio) were obtained from a local commercial distributor (ZooMix, Barnaul, Russia) and housed in groups of 100 fish per 50-L tank filled with filtered system water maintained at 25 °C (pH 7.8–8.0, 470–490 ms/mL). Illumination (590–600 lx) was provided by 36 ceiling-mounted 18-Wt fluorescent light tubes with a 12/12 light/dark cycle

Journal Pre-proofs
according to the standards of zebrafish care [80]. All fish used in this study were experimentally naive and fed twice daily with Tetramin-Pro (Terta GMBH, Osnabruck, Germany). Animal experiments were approved by the IACUC of the N.D. Zelinsky Institute of Organic Chemistry and fully adhered to the National and Institutional guidelines and regulations.

Behavioral testing and pharmacological manipulations [47]. Behavioral testing was performed between 11.00 and 18.00 h using tanks with water adjusted to the holding room temperature to assess zebrafish behavior in the novel tank test. Prior to testing, fish were pre-exposed in a 0.5-L plastic beaker for 20 min to either a drug-treated or drug-free vehicle, 0.1% solution of dimethyl sulfoxide (DMSO, Acrus, Moscow, Russia) known to be devoid of own behavioral effects in zebrafish, and is commonly used in zebrafish drug studies (10 fish in group) [81]. The standard 20-min pre-treatment time and 1 mg/L doses were chosen based on experience with various CNS drugs. Zolpidem was used as the reference drug. Fish were then exposed to the novel tank test, assessing their anxiety and locomotion [49, 82]. The tank consisted of a 1.8-L rectangle tank (15 cm height × 20 cm length × 6 cm width) filled with water up to 14.5 cm height and divided into two equal virtual horizontal portions by a line marking the outside walls. Trials were recorded by front and top web-cameras for further analyses. The standard video recording time for the experiment was 6 min. Zebrafish behavior was then processed by a trained observer, blinded to the treatments, to manually score different behavioral endpoints (intra-rater reliability > 0.85), such as the time spent in top, top entries, the latency to top entry (s), the number and duration (s) of freezing bouts, the number of complete, erratic movements and erratic bottom movements. Freezing was defined as the total absence of movement, except for the gills and eyes, for > 2 s. In experiments on withdrawal of behavioral effects, Flumazenil was used as a 1.0 mg/L water solution with the 10-min treatment time.

Statistical analyses. Behavioral data were analyzed using the Kruskal–Wallis test followed by Dunn's post-hoc tes, and expressed as mean ± SEM (n = 10 per group). All experimenters were blinded to the treatments. All tested animals were included in final analyses without attrition or exclusion, and all planned analyses were reported here. Statistical significance was set at $P < 0.05$ in all tests.

Toxicity. The fish were exposed to the tested substance preferably for 96 h. Mortalities were recorded at 24, 48, 72, and 96 h, and the concentrations, which killed 50% of the fish (LC_{50}), were determined where possible. One or more species may be used, the choice being at the discretion of the testing laboratory. At least seven fishes were used at each test concentration (starting from 1.0 mg/L) and in the controls. The tested substances were administered to, at least, five concentrations in a geometric series with a factor preferably not exceeding 2.2. The limit test corresponds to one dose level of 100 mg/L. The cumulative percentage mortality for each exposure period was plotted against the concentration on logarithmic probability paper.

Animal experiments were approved by the IACUC of V. V. Zakusov Institute of Pharmacology and fully adhered to the National and Institutional guidelines and regulations.

Electrophysiological studies

Journal Pre-proofs

Preparation of Purkinje cells. All experiments were conducted in accordance with the requirements of the Ministry of Public Health of the Russian Federation and were consistent with EU directive for Use of Experimental Animals of the European Community. Maximum efforts were made to minimize both the number and sufferings of used animal.

Dissociated neurons were prepared from 13~16-day-old Wistar rats by a method described previously [83]. Briefly, after decapitation the brain was removed and sagittal slices of the cerebellum 200-500 μm thick were cut with a razor blade and incubated at room temperature for 2–6 h. The incubation solution consisted of (in mM): NaCl, 124; KCl, 3; $CaCI_2$, 2; $MgSO_4$, 2; NaH_2PO_4, 1.3; $NaHCO_3$, 25; D-glucose, 10, pH 7.4. The saline was continuously stirred and bubbled with carbogen (95% O_2 + 5% CO_2). One at a time, slices were transferred to the recording chamber and neurons were isolated by vertical vibration of a glass sphere, ~0.7 mm in diameter, placed close to the surface of the slice [83]. The dissociated cells settled on the bottom of the chamber, from where they were picked up with a patch pipette. Manipulations and cell identification were performed using an inverted microscope. Isolated Purkinje cells were distinguished from other cerebellar cells based on their large cell bodies (approximately 20 μm) and characteristic pear shape attributable to the stumps of the apical dendrites. The solution for dissociation and recording had the following composition: NaCl, 150; KCl, 5; $CaCl_2$, 2.7; $MgCl_2$, 2.0; HEPES, 10, pH adjusted to 7.4 with NaOH.

Whole-cell recording. Voltage-clamp recording was performed using the whole-cell configuration of the patch-clamp technique [84]. Glass recording patch pipettes were prepared from filament-containing borosilicate tubes using a two-stage puller. The electrodes, having resistance of 2–2.5 MOhm, were filled with a recording solution of the following composition (in mM): CsCl, 100; CsF, 40; $CaCl_2$, 0.5; $MgCl_2$, 4; HEPES, 10; EGTA, 5; ATP-Na, 4 (pH adjusted to 7.2 with CsOH). Recordings were carried out at room temperature (20–23°C) using an EPC 7 patch-clamp amplifier. Currents were filtered at 3 kHz, sampled at 10kHz, and stored on a computer disk. Cells were held at a membrane potential of –70 mV.

Drug solutions and drug application. A fast perfusion system was used for solution exchange [85]. Isolated Purkinje cells were first patch-clamped and then lifted into the application system, where they were continuously perfused with a control bath solution. The substances were applied through a glass capillarie ~0.2 mm in diameter, which could be rapidly laterally displaced. For drug exposure, the perfusion system was laterally moved to place the cell in the solution stream. The system allows a complete exchange of external solution surrounding a neuron within 20 ms. For activation of $GABA_AR$, in most experiments GABA was applied over periods of 2 s, at 40–60 s intervals.

Data processing. Whole-cell records were analyzed off-line being exported as text files to Prism (GraghPad Software, San Diego, CA) for further analysis. GABA concentration–response relationships were fitted to the equation $I/I_{max}=[GABA]^{nH}/(EC_{50}{}^{nH}+[GABA]^{nH})$ (Equation 1), where I and I_{max} represent the normalized GABA-induced current at a given concentration and the maximum current induced by a saturating concentration of GABA, respectively, EC_{50} is 50% effective GABA concentration, and nH is the Hill coefficient.

Journal Pre-proofs

Concentration-response curves for the tested substances were generated by applying a series of concentrations of these compounds in the presence of 2 μM GABA. The data at a given concentration of the tested compounds were averaged across all cells, and the averaged data were fitted with curves. The enhancement of the GABA-gated Cl^- current (I_{GABA}) was defined as $B = 1+ A/((1 + (EC^{BZ}_{50}/[BZ])^{nH}))$ (Equation 2), were $B = I_{GABA+BZ}\ I_{GABA}$ is the degree of potentiation of GABA (2 μM) current induced by the tested compounds (BZ), A is the maximum peak current in the presence of a modulator, EC^{BZ}_{50} is the concentration of the BZ compound that produces a response equal to 50% of the maximum current, *nH* is the Hill coefficient.

Statistical analysis. Statistical analysis and curve fitting were performed using the *Prism Graphpad* software. All comparisons were made with a paired two-tailed *t*-test. In the description of results, mean and standard error of mean (SEM) are specified. In the figures, error bars represent SEM.

Molecular modeling

*Homology modeling***.** We built a model of open α1β2γ2 $GABA_AR$ with 2:2:1 subunit stoichiometry. As a prototype for $GABA_AR$ building, we used the cryo-EM structure of homo-oligomeric α1 GlyR [86] corresponding to the open channel state. GlyR is a close homolog of $GABA_AR$. Therefore, the structure of GlyR is well suited for $GABA_AR$ modeling. Initial alignment was done using Clustal Omega [87] and then manually refined based on experimental data. In the extracellular domain (ECD) of $GABA_AR$, regions of the most uncertain alignment include the loops F and C. The loop F is the main area of manual refinement. Sancar, Ericksen, Kucken, Teissere and Czajkowski [62] showed that the residues Glu189 and Arg194 of the γ2 subunit are essential for BZD binding. In our alignment, the side chains of these residues face toward the BZD binding site. The alignment of the loops F and C is shown in Figure S2 B.

Model building. The starting backbone geometry of the $GABA_AR$ model was taken from the template structure. The side chain torsions in those residues, which are identical in the template and model, were assigned starting values as in the template. All-trans conformations were used as the initial approximation for the side chains of residues that mismatched between the model and template. The Monte Carlo energy minimization (MCM) method [88] was applied to optimize the $GABA_AR$ model. Energy was minimized in generalized coordinate space using the ZMM program (http://www.zmmsoft.com).

Nonbonded interactions were calculated using the AMBER force field [89] with a cutoff distance of 9 Å. Electrostatic interactions were calculated with the solvent exposure- and distance-dependent dielectric function [90] without cutoff for interactions involving ionized groups. The MCM protocol was performed in two stages. In the first stage, the energy was MC-minimized with constraints. The C_α atoms in the model were constrained to the corresponding positions in the template with a help of pins. A pin is a flat-bottom penalty function [91] that allows penalty-free deviations of the respective atom up to 1 Å from the template and imposes an energy penalty for larger deviations. After the convergence of the constrained MCM trajectory, all constraints were removed and the model was refined by the unconstrained MCM procedure. Each MCM

Journal Pre-proofs
trajectory was terminated when 10,000 consecutive energy minimizations did not improve the energy of the apparent global minimum. The difference between structures found in the constrained and unconstrained trajectories indicated whether the constrained search yielded a stable structure.

Ligand docking. The ligand molecules were built with the MOE computer program (Figure 6A). The MCM method was applied to find the lowest energy conformations of the molecules. Geometry of this compound was optimized using the HGRID (Hot GRID) procedure that submits a large number of MCM trajectories from randomly generated starting points and collects low-energy structures found in each trajectory [92]. The bond angles at all heavy atoms of the ligand were allowed to vary during energy minimization. The atomic charges of the ligand were calculated by the AM1 method[93] using the MOPAC program.
The MCM protocol allows finding energetically optimal ligand receptor complexes by varying the position and orientation of the ligand, as well as the torsion angles of the ligand and the surrounding amino acid side chains. This search was carried within a certain area around the starting position of the ligand. It is known that the BZD binding site is located at the α(+)/γ(-) intersubunit interface in ECD [64]. The tested ligands were manually docked in the BZB binding site. The search of the optimal mode of the ligands binding was performed in two steps. In the first step, the distant constraints were imposed on the ligand. This trajectory relaxed bad ligand–receptor contacts that inevitably emerged at the manual docking. The structure obtained in the first MCM trajectory was used as the starting point for the second one, in which all constraints were removed. Each MCM trajectory was terminated when the last 5,000 consecutive energy minimizations did not improve the energy.

AUTHOR INFORMATION

*Address: N. D. Zelinsky Institute of Organic Chemistry, Russian Academy of Sciences, 47 Leninsky prosp., 119991 Moscow, Russia. Phone: +7 (903) 540-74-78, E-mail: yavolkova@gmail.com.

ORCID

Tatyana A. Tikhonova 0000-0003-2472-6124

Julia V. Bukanova 0000-0001-8961-8760

Alexey V. Rossokhin 0000-0001-7024-7461

Irina N. Sharonova 0000-0001-9955-1870

Georgy I. Kovalev 0000-0002-8597-7018

Igor V. Zavarzin 0000-0002-8194-5756

Yulia A. Volkova 0000-0001-8554-838X

NOTES

The authors declare no competing financial interest. All authors were employed by Eli Lilly and Company during time this research was conducted.

ACKNOWLEDGMENT

The research was carried out using the equipment of the shared research facilities of HPC computing resources at the Lomonosov Moscow State University. This work was supported by the RFBR grant 18-33-20087 (chemistry, biological studies, molecular modeling) and 18-015-00038 (molecular modeling).

ABBREVIATIONS USED

GABA, γ-aminobutyric acid; CNS, central nervous system; $GABA_ARs$, γ-aminobutyric acid type A receptors; PAMs, positive allosteric modulators; BZDs, benzodiazepines; FDA, Food and Drug Administration; ZLP, Zolpidem; DZP, Diazepam; ECD, extracellular domain; MEC, minimal energy conformation.

KEYWORDS

positive allosteric modulators, $GABA_A$ receptors, imidazopyridine drugs, imidazo[2,1-b]thiazoles, imidazo[2,1-b][1,3,4]thiadiazoles, benzo[d]imidazo[2,1-b]thiazoles, benzodiazepine-binding site.

REFERENCES

[1] M. Chebib, G.A.R. Johnston, GABA-Activated Ligand Gated Ion Channels: Medicinal Chemistry and Molecular Biology, J. Med. Chem. 43(8) (2000) 1427-1447.

[2] E. Sigel, M.E. Steinmann, Structure, function, and modulation of GABA(A) receptors, J. Biol. Chem. 287(48) (2012) 40224-40231.

[3] P.J. Whiting, GABA-A receptor subtypes in the brain: a paradigm for CNS drug discovery?, Drug Discov. Today 8(10) (2003) 445-450.

[4] S.J. Farrar, P.J. Whiting, T.P. Bonnert, R.M. McKernan, Stoichiometry of a ligand-gated ion channel determined by fluorescence energy transfer, J. Biol. Chem. 274(15) (1999) 10100-10104.

[5] R.M. McKernan, P.J. Whiting, Which GABAA-receptor subtypes really occur in the brain?, Trends Neurosc. 19(4) (1996) 139-143.

[6] V. Tretter, N. Ehya, K. Fuchs, W. Sieghart, Stoichiometry and assembly of a recombinant GABAA receptor subtype, J. Neurosc. 17(8) (1997) 2728-2737.

[7] M. Farrant, Z. Nusser, Variations on an inhibitory theme: phasic and tonic activation of GABA A receptors, Nature Rev. Neurosc. 6(3) (2005) 215.

Journal Pre-proofs
[8] R.W. Olsen, W. Sieghart, $GABA_A$ receptors: subtypes provide diversity of function and pharmacology, Neuropharmacology 56(1) (2009) 141-148.

[9] R.W. Olsen, Chapter Seven - Allosteric ligands and their binding sites define γ-aminobutyric acid (GABA) type A receptor subtypes, Adv. Pharmacol. Academic Press 2015, pp. 167-202.

[10] M. Seifi, J.F. Brown, J. Mills, P. Bhandari, D. Belelli, J.J. Lambert, U. Rudolph, J.D. Swinny, Molecular and functional diversity of GABA-A receptors in the enteric nervous system of the mouse colon, J. Neurosc. 34(31) (2014) 10361-10378.

[11] R. Puthenkalam, M. Hieckel, X. Simeone, C. Suwattanasophon, R.V. Feldbauer, G.F. Ecker, M. Ernst, Structural Studies of $GABA_A$ Receptor Binding Sites: Which Experimental Structure Tells us What?, Front. Mol. Neurosc. 9 (2016) 44-44.

[12] W. Sieghart, J. Ramerstorfer, I. Sarto-Jackson, Z. Varagic, M. Ernst, A novel GABA(A) receptor pharmacology: drugs interacting with the α(+) β(-) interface, Br. J. Pharmacol. 166(2) (2012) 476-485.

[13] S. Oakley, L.S. Vedula, W. Bu, Q.C. Meng, J. Xi, R. Liu, R.G. Eckenhoff, P.J. Loll, Recognition of anesthetic barbiturates by a protein binding site: a high resolution structural analysis, PloS One 7(2) (2012) e32070.

[14] S.J. Middendorp, M.C. Maldifassi, R. Baur, E. Sigel, Positive modulation of synaptic and extrasynaptic GABAA receptors by an antagonist of the high affinity benzodiazepine binding site, Neuropharmacology 95 (2015) 459-467.

[15] Z.-W. Chen, J. Bracamontes, W.W. Cheng, M. Budelier, K. Kathiresan, M. Qian, D.F. Covey, A.S. Evers, Identification of Neurosteroid Binding Sites on $GABA_A$ Receptors using Photolabeling with Mass Spectrometry, Biophys. J. 114(3) (2018) 25a.

[16] D. Laverty, P. Thomas, M. Field, O.J. Andersen, M.G. Gold, P.C. Biggin, M. Gielen, T.G. Smart, Crystal structures of a GABA A-receptor chimera reveal new endogenous neurosteroid-binding sites, Nature Struct. Mol. Biol. 24(11) (2017) 977.

[17] A. Estrada, J. Lynch, Functional characterization of ivermectin binding sites in α1β2γ2L GABA (A) receptors, Front. Mol. Neurosc. 8 (2015) 55.

[18] H. Möhler, J. Fritschy, U. Rudolph, A new benzodiazepine pharmacology, J. Pharm. Exp. Ther. 300(1) (2002) 2-8.

[19] E. Sigel, M. Ernst, The benzodiazepine binding sites of $GABA_A$ receptors, Trends Pharmacol. Sci. 39(7) (2018) 659-671.

[20] R. Puthenkalam, M. Hieckel, X. Simeone, C. Suwattanasophon, R.V. Feldbauer, G.F. Ecker, M. Ernst, Structural studies of GABAA receptor binding sites: which experimental structure tells us what?, Front. Mol. Neurosc. 9 (2016) 44.

Journal Pre-proofs
[21] T. Kishi, K. Inada, Y. Matsui, N. Iwata, Z-drug for schizophrenia: A systematic review and meta-analysis, Psychiatry Res. 256 (2017) 365-370.

[22] K. Donnelly, R. Bracchi, J. Hewitt, P.A. Routledge, B. Carter, Benzodiazepines, Z-drugs and the risk of hip fracture: A systematic review and meta-analysis, PloS One 12(4) (2017) e0174730.

[23] J. Brandt, C. Leong, Benzodiazepines and Z-drugs: an updated review of major adverse outcomes reported on in epidemiologic research, Drugs in R&D 17(4) (2017) 493-507.

[24] M.J.L. Rivilli, A.V. Turina, E.A. Bignante, V.H. Molina, M.A. Perillo, M.C. Briñon, E.L. Moyano, Synthesis and pharmacological evaluation of pyrazolo [4, 3-c] quinolinones as high affinity GABAA-R ligands and potential anxiolytics, Bioorg. Med. Chem. 26(14) (2018) 3967-3974.

[25] T.D. Prevot, G. Li, A. Vidojevic, K.A. Misquitta, C. Fee, A. Santrac, D.E. Knutson, M.R. Stephen, R. Kodali, N.M. Zahn, Novel Benzodiazepine-Like Ligands with Various Anxiolytic, Antidepressant, or Pro-Cognitive Profiles, Mol. Neuropsychiatry 5(2) (2019) 84-97.

[26] S.C. Goodacre, L.J. Street, D.J. Hallett, J.M. Crawforth, S. Kelly, A.P. Owens, W.P. Blackaby, R.T. Lewis, J. Stanley, A.J. Smith, Imidazo [1, 2-a] pyrimidines as functionally selective and orally bioavailable GABAAα2/α3 binding site agonists for the treatment of anxiety disorders, J. Med. Chem. 49(1) (2006) 35-38.

[27] P. Skolnick, Anxioselective anxiolytics: on a quest for the Holy Grail, Trends Pharmacol. Sci. 33(11) (2012) 611-620.

[28] R. Sankar, GABA A receptor physiology and its relationship to the mechanism of action of the 1, 5-benzodiazepine clobazam, CNS drugs 26(3) (2012) 229-244.

[29] K. Yakoub, S. Jung, C. Sattler, H. Damerow, J. Weber, A. Kretzschmann, A.S. Cankaya, M. Piel, F. Rösch, A.S. Haugaard, B. Frølund, T. Schirmeister, H. Lüddens, Structure–Function Evaluation of Imidazopyridine Derivatives Selective for δ-Subunit-Containing γ-Aminobutyric Acid Type A ($GABA_A$) Receptors, J. Med. Chem. 61(5) (2018) 1951-1968.

[30] N. Denora, V. Laquintana, M.G. Pisu, R. Dore, L. Murru, A. Latrofa, G. Trapani, E. Sanna, 2-Phenyl-imidazo [1, 2-a] pyridine compounds containing hydrophilic groups as potent and selective ligands for peripheral benzodiazepine receptors: synthesis, binding affinity and electrophysiological studies, J. Med. Chem. 51(21) (2008) 6876-6888.

[31] J. Koubachi, S. El Kazzouli, S. Berteina-Raboin, A. Mouaddib, G. Guillaumet, Synthesis of polysubstituted imidazo [1, 2-a] pyridines *via* microwave-assisted one-pot cyclization/Suzuki coupling/palladium-catalyzed heteroarylation, J. Org. Chem. 72(20) (2007) 7650-7655.

Journal Pre-proofs
[32] A. Trabanco, G. Tresadern, G.J. Macdonald, J.A. Vega, A.I. de Lucas, E.n. Matesanz, A.n. García, M.L. Linares, S.A. Alonso de Diego, J.M. Alonso, Imidazo [1, 2-a] pyridines: orally active positive allosteric modulators of the metabotropic glutamate 2 receptor, J. Med. Chem. 55(6) (2012) 2688-2701.

[33] E. Mignot, The perfect hypnotic?, Science 340(6128) (2013) 36-38.

[34] A. Noormandi, M. Shahrokhi, H. Khalili, Potential benefits of zolpidem in disorders of consciousness, Exp. Rev. Clin. Pharm. 10(9) (2017) 983-992.

[35] K.A. Wafford, M.B. van Niel, Q.P. Ma, E. Horridge, M.B. Herd, D.R. Peden, D. Belelli, J.J. Lambert, Novel compounds selectively enhance δ subunit containing GABAA receptors and increase tonic currents in thalamus, Neuropharmacology 56(1) (2009) 182-189.

[36] M. Jensen, K. Wafford, A. Brown, D. Belelli, J. Lambert, N. Mirza, A study of subunit selectivity, mechanism and site of action of the delta selective compound 2 (DS2) at human recombinant and rodent native $GABA_A$ receptors, Br. J. Pharmacol. 168(5) (2013) 1118-1132.

[37] A.C. Altamura, D. Moliterno, S. Paletta, M. Maffini, M.C. Mauri, S. Bareggi, Understanding the pharmacokinetics of anxiolytic drugs, Expert Opin. Drug Metab. Toxicol. 9(4) (2013) 423-440.

[38] L.S. Heidelberg, J.W. Warren, J.L. Fisher, SB-205384 is a positive allosteric modulator of recombinant $GABA_A$ receptors containing rat α3, α5, or α6 subunit subtypes coexpressed with β3 and γ2 subunits, J. Pharmacol. Exp. Therapeutics 347(1) (2013) 235-241.

[39] F. Palagiano, L. Arenare, P.C. De, G. Grandolini, V. Ambrogi, L. Perioli, W. Filippelli, G. Falcone, F. Rossi, Synthesis and SAR study of imidazo [2, 1-b] benzothiazole acids and some related compounds with anti-inflammatory and analgesic activities, Farmaco 51(7) (1996) 483-491.

[40] M. Sevrin, C. Morel, M. Mangane, P. George, 2-thienylimidazo [2, 1-β] benzothiazole-3-acetic acid derivatives, their preparation and their use, 1995, US5418248A.

[41] El-Shorbagi, A. N.; Sakai, S.; el-Gendy, M. A.; Omar, N.; Farag, H. H. Imidazo [2,1-b] benzothiazoles. I, Chem. Pharm. Bull. 36 (1988) 4760-4768.

[42] M. Marcinkowska, M. Kołaczkowski, K. Kamiński, A. Bucki, M. Pawłowski, A. Siwek, T. Karcz, B. Mordyl, G. Starowicz, P. Kubowicz, Design, synthesis, and biological evaluation of fluorinated imidazo [1, 2-a] pyridine derivatives with potential antipsychotic activity, Eur. J. Med. Chem. 124 (2016) 456-467.

[43] I.V. Rassokhina, V.Z. Shirinian, I.V. Zavarzin, V. Gevorgyan, Y.A. Volkova, Copper (II)-mediated aerobic synthesis of imidazo [1,2-a] pyridines *via* cascade aminomethylation/cycloisomerization of alkynes, J. Org. Chem. 80(21) (2015) 11212-11218.

Journal Pre-proofs
[44] I.V. Kassokhina, T.A. Tikhonova, S.G. Kobylskoy, T.Y. Babkin, V.Z. Shirinian, V. Gevorgyan, I.V. Zavarzin, Y.A. Volkova, Synthesis of Imidazo [2, 1-b] thiazoles *via* Copper-Catalyzed A^3-Coupling in Batch and Continuous Flow, J. Org. Chem. 82(18) (2017) 9682-9692.

[45] P. Panula, V. Sallinen, M. Sundvik, J. Kolehmainen, V. Torkko, A. Tiittula, M. Moshnyakov, P. Podlasz, Modulatory neurotransmitter systems and behavior: towards zebrafish models of neurodegenerative diseases, Zebrafish 3(2) (2006) 235-247.

[46] Z. Bencan, D. Sledge, E.D. Levin, Buspirone, chlordiazepoxide and diazepam effects in a zebrafish model of anxiety, Pharmacol. Biochem. Behav. 94(1) (2009) 75-80.

[47] J. Cachat, A. Stewart, L. Grossman, S. Gaikwad, F. Kadri, K.M. Chung, N. Wu, K. Wong, S. Roy, C. Suciu, Measuring behavioral and endocrine responses to novelty stress in adult zebrafish, Nature Prot. 5(11) (2010) 1786-1799.

[48] C. Maximino, T.M. de Brito, A.W. da Silva Batista, A.M. Herculano, S. Morato, A. Gouveia Jr, Measuring anxiety in zebrafish: a critical review, Behav. Brain Res. 214(2) (2010) 157-171.

[49] Y. Nishimura, S. Okabe, S. Sasagawa, S. Murakami, Y. Ashikawa, M. Yuge, K. Kawaguchi, R. Kawase, T. Tanaka, Pharmacological profiling of zebrafish behavior using chemical and genetic classification of sleep-wake modifiers, Front. Pharmacol. 6 (2015) 257.

[50] M.J.S. Dewar, E.G. Zoebisch, E.F. Healy, J.J.P. Stewart, AM1: A new general purpose quantum mechanical molecular model, J. Am. Chem. Soc. 107 (1985) 3902-3909.

[51 The exception was compound **34** with IC_{50} = 198 nM

[52] E. Sigel, R. Baur, Allosteric modulation by benzodiazepine receptor ligands of the $GABA_A$ receptor channel expressed in Xenopus oocytes, J. Neuroscience 8(1) (1988) 289-295.

[53] https://www.oecd-ilibrary.org/environment/test-no-203-fish-acute-toxicity-test_9789264069961-en.

[54] D. Laurie, W. Wisden, P. Seeburg, The distribution of thirteen GABAA receptor subunit mRNAs in the rat brain. III. Embryonic and postnatal development, J. Neuroscience 12(11) (1992) 4151-4172.

[55] J.M. Fritschy, H. Mohler, GABAA-receptor heterogeneity in the adult rat brain: differential regional and cellular distribution of seven major subunits, J. Compar. Neurology 359(1) (1995) 154-194.

[56] V. Itier, H. Depoortere, B. Scatton, P. Avenet, Zolpidem functionally discriminates subtypes of native $GABA_A$ receptors in acutely dissociated rat striatal and cerebellar neurons, Neuropharmacology 35(2) (1996) 137-145.

Journal Pre-proofs
[57] C. Sur, K.A. Wafford, D.S. Reynolds, K.L. Hadingham, F. Bromidge, A. Macaulay, N. Collinson, G. O'Meara, O. Howell, R. Newman, Loss of the major $GABA_A$ receptor subtype in the brain is not lethal in mice, J. Neuroscience 21(10) (2001) 3409-3418.

[58] A. Buhr, R. Baur, E. Sigel, Subtle changes in residue 77 of the gamma subunit of alpha1beta2gamma2 $GABA_A$ receptors drastically alter the affinity for ligands of the benzodiazepine binding site, J. Biol. Chem. 272(18) (1997) 11799-804.

[59] A. Buhr, E. Sigel, A point mutation in the gamma2 subunit of gamma-aminobutyric acid type A receptors results in altered benzodiazepine binding site specificity, Proc. Natl. Acad. Sci. U.S.A. 94(16) (1997) 8824-8829.

[60] P.B. Wingrove, S.A. Thompson, K.A. Wafford, P.J. Whiting, Key Amino Acids in the γ Subunit of the γ-Aminobutyric AcidA Receptor that Determine Ligand Binding and Modulation at the Benzodiazepine Site, Mol. Pharmacol. 52(5) (1997) 874-881.

[61] S.M. Hanson, E.V. Morlock, K.A. Satyshur, C. Czajkowski, Structural requirements for eszopiclone and zolpidem binding to the gamma-aminobutyric acid type-A ($GABA_A$) receptor are different, J. Med. Chem. 51(22) (2008) 7243-7252.

[62] F. Sancar, S.S. Ericksen, A.M. Kucken, J.A. Teissere, C. Czajkowski, Structural determinants for high-affinity zolpidem binding to GABA-A receptors, Mol. Pharmacol. 71(1) (2007) 38-46.

[63] S. Masiulis, R. Desai, T. Uchanski, I. Serna Martin, D. Laverty, D. Karia, T. Malinauskas, J. Zivanov, E. Pardon, A. Kotecha, J. Steyaert, K.W. Miller, A.R. Aricescu, $GABA_A$ receptor signalling mechanisms revealed by structural pharmacology, Nature 565 (2019), 454–459.

[64] W. Sieghart, Allosteric Modulation of GABAA Receptors via Multiple Drug-Binding Sites, Adv. Pharmacol. 72 (2015) 53-96.

[65] T. Palani, K. Park, M.R. Kumar, H.M. Jung, S. Lee, Copper-Catalyzed Decarboxylative Three-Component Reactions for the Synthesis of Imidazo [1, 2-a] pyridines, Eur. J. Org. Chem. 2012(26) (2012) 5038-5047.

[66] H. Möhler, M. Battersby, J. Richards, Benzodiazepine receptor protein identified and visualized in brain tissue by a photoaffinity label, Proc. Natl. Acad. Sci. U.S.A. 77(3) (1980) 1666-1670.

[67] E. Barnard, P. Skolnick, R. Olsen, H. Mohler, W. Sieghart, G. Biggio, C. Braestrup, A. Bateson, S. Langer, Subtypes of gamma-aminobutyric acid A receptors: classification on the basis of subunit structure and receptor function, Pharmacol Rev. 50(2) (1998) 291-313.

Journal Pre-proofs
[68] U. Rudolph, H. Möhler, Analysis of GABAA receptor function and dissection of the pharmacology of benzodiazepines and general anesthetics through mouse genetics, Annu. Rev. Pharmacol. Toxicol. 44 (2004) 475-498.

[69] P.J. Whiting, GABA-A receptors: a viable target for novel anxiolytics?, Curr. Opin. Pharmacol. 6(1) (2006) 24-29.

[70] H. Möhler, F. Crestani, U. Rudolph, GABAA-receptor subtypes: a new pharmacology, Curr. Opin. Pharmacol. 1(1) (2001) 22-25.

[71] B.D. Fontana, N.J. Mezzomo, A.V. Kalueff, D.B. Rosemberg, The developing utility of zebrafish models of neurological and neuropsychiatric disorders: A critical review, Exp. Neurology 299 (2018) 157-171.

[72] K. Howe, M.D. Clark, C.F. Torroja, J. Torrance, C. Berthelot, M. Muffato, J.E. Collins, S. Humphray, K. McLaren, L. Matthews, The zebrafish reference genome sequence and its relationship to the human genome, Nature 496(7446) (2013) 498-503.

[73] A.C.V. Giacomini, M.S. Abreu, L.V. Giacomini, A.M. Siebel, F.F. Zimerman, C.L. Rambo, R. Mocelin, C.D. Bonan, A.L. Piato, L.J. Barcellos, Fluoxetine and diazepam acutely modulate stress induced-behavior, Behav. Brain Res. 296 (2016) 301-310.

[74] E.V. Kysil, D.A. Meshalkina, E.E. Frick, D.J. Echevarria, D.B. Rosemberg, C. Maximino, M.G. Lima, M.S. Abreu, A.C. Giacomini, L.J. Barcellos, Comparative analyses of zebrafish anxiety-like behavior using conflict-based novelty tests, Zebrafish 14(3) (2017) 197-208.

[75] D.B. Rosemberg, M.M. Braga, E.P. Rico, C.M. Loss, S.D. Córdova, B.H.M. Mussulini, R.E. Blaser, C.E. Leite, M.M. Campos, R.D. Dias, Behavioral effects of taurine pretreatment in zebrafish acutely exposed to ethanol, Neuropharmacol. 63(4) (2012) 613-623.

[76] B. Monesson-Olson, J.J. McClain, A.E. Case, H.E. Dorman, D.R. Turkewitz, A.B. Steiner, G.B. Downes, Expression of the eight $GABA_A$ receptor α subunits in the developing zebrafish central nervous system, PloS one 13(4) (2018) e0196083.

[77] J.K. Gill-Thind, P. Dhankher, J.M. D'Oyley, T.D. Sheppard, N.S. Millar, Structurally similar allosteric modulators of alpha7 nicotinic acetylcholine receptors exhibit five distinct pharmacological effects, J. Biol. Chem. 290(6) (2015) 3552-62.

[78] J.S. Oakdale, R.K. Sit, V.V. Fokin, Ruthenium-catalyzed cycloadditions of 1-haloalkynes with nitrile oxides and organic azides: synthesis of 4-haloisoxazoles and 5-halotriazoles, Chemistry 20(35) (2014) 11101-11110.

[79] J.B. Baell, G.A. Holloway, New substructure filters for removal of pan assay interference compounds (PAINS) from screening libraries and for their exclusion in bioassays, J. Med. Chem. 53(7) (2010) 2719-2740.

Journal Pre-proofs
[80] Westerfield, The Zebrafish Book University of Oregon Press Eugene, 2000, 4-5.
[81] P. Goldsmith, Zebrafish as a pharmacological tool: the how, why and when, Curr. Opin. Pharmacol. 4(5) (2004) 504-512.
[82] A.V. Kalueff, D.J. Echevarria, S. Homechaudhuri, A.M. Stewart, A.D. Collier, A.A. Kaluyeva, S. Li, Y. Liu, P. Chen, J. Wang, Zebrafish neurobehavioral phenomics for aquatic neuropharmacology and toxicology research, Aquat. Toxicol. 170 (2016) 297-309.
[83] V.S. Vorobjev, Vibrodissociation of sliced mammalian nervous tissue, J. Neuroscience Methods 38(2-3) (1991) 145-150.
[84] O.P. Hamill, A. Marty, E. Neher, B. Sakmann, F.J. Sigworth, Improved patch-clamp techniques for high-resolution current recording from cells and cell-free membrane patches, Eur. J. Physiol. 391(2) (1981) 85-100.
[85] V.S. Vorobjev, I.N. Sharonova, H.L. Haas, A simple perfusion system for patch-clamp studies, J. Neuroscience Methods 68(2) (1996) 303-307.
[86] J. Du, W. Lu, S. Wu, Y. Cheng, E. Gouaux, Glycine receptor mechanism elucidated by electron cryo-microscopy, Nature 526(7572) (2015) 224-229.
[87] F. Sievers, A. Wilm, D. Dineen, T.J. Gibson, K. Karplus, W. Li, R. Lopez, H. McWilliam, M. Remmert, J. Soding, J.D. Thompson, D.G. Higgins, Fast, scalable generation of high-quality protein multiple sequence alignments using Clustal Omega, Mol. Syst. Biol. 7 (2011) 539.
[88] Z. Li, H.A. Scheraga, Monte Carlo-minimization approach to the multiple-minima problem in protein folding, Proc. Natl. Acad. Sci. U.S.A. 84(19) (1987) 6611-5.
[89] J. Weiner, P.A. Kollman, D.A. Case, U.C. Singh, C. Chio, G. Alagona, S. Profeta, P.K. Weiner, A new force field for molecular mechanical simulation of nucleic acids and proteins, J. Am. Chem. Soc. 106 (1984) 765-784.
[90] D.P. Garden, B.S. Zhorov, Docking flexible ligands in proteins with a solvent exposure- and distance-dependent dielectric function, J. Comput. Aid. Mol. Des. 24(2) (2010) 91-105.
[91] C.L. Brooks, B.M. Pettitt, M. Karplus, Structural and energetic effects of truncating long ranged interactions in ionic polar fluids., J. Chem. Phys. 83 (1985) 5897-5908.
[92] A. Rossokhin, G. Teodorescu, S. Grissmer, B.S. Zhorov, Interaction of d-tubocurarine with potassium channels: molecular modeling and ligand binding, Mol. Pharmacol. 69(4) (2006) 1356-1365.
[93] E. Zoebisch, E. Healy, J. Stewart, AM1: A new general purpose quantum mechanical model, J. Am. Chem. Soc. 107 (1985) 3902-3909.

Table of Contents Graphic

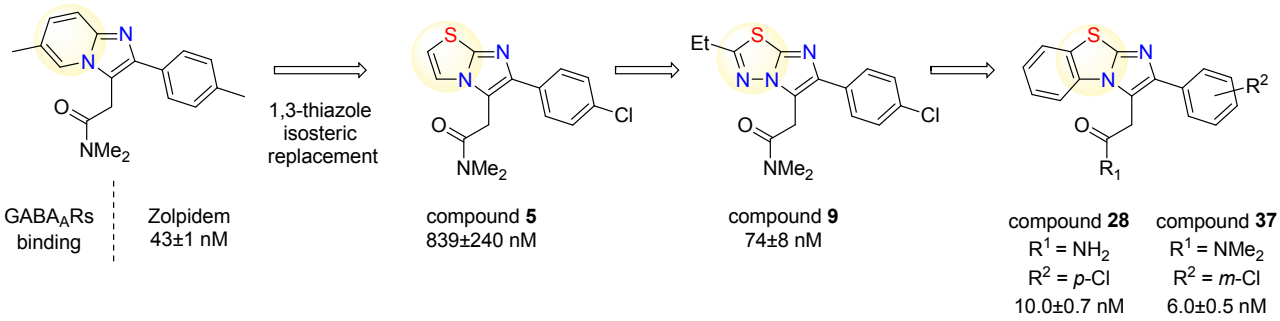

Journal Pre-proofs

Highlights

- Three series of novel γ-aminobutyric acid receptor ($GABA_AR$) positive allosteric modulators (PAMs) derived by 1,3-thiazole isosteric replacement in imidazopyridine drugs were designed.
- In each of these series (imidazo[2,1-b]thiazoles, imidazo[2,1-b][1,3,4]thiadiazoles, and benzo[d]imidazo[2,1-b]thiazoles) lead compounds were discovered using a radioligand competition binding assay.
- A number of benzo[d]imidazo[2,1-b]thiazoles exhibited affinity for $GABA_ARs$ benzodiazepine binding site 3 – 7 times lower to the reference drug Zolpidem.
- The functional properties of highest-affinity compounds **28** and **37** as $GABA_AR$ PAMs were determined by electrophysiological measurements.
- Biological efficacy of benzo[d]imidazo[2,1-b]thiazoles was demonstrated *in vivo* in behavioral assays using zebrafish as experimental animals.
- Active compounds were safe and non-toxic.
- Structural basis for activity of benzo[d]imidazo[2,1-b]thiazoles were proposed using extensive molecular docking studies.

Journal Pre-proofs